

See discussions, stats, and author profiles for this publication at: <https://www.researchgate.net/publication/51991272>

Synthesis and Structural and Spectroscopic Characterization of Mononuclear Copper Nitrosyl Complexes: Models for Nitric Oxide Adducts of Copper Proteins and Copper-Exchanged Zeolit...

ARTICLE *in* JOURNAL OF THE AMERICAN CHEMICAL SOCIETY · DECEMBER 1993

Impact Factor: 12.11 · DOI: 10.1021/ja00077a030

CITATIONS

129

READS

11

6 AUTHORS, INCLUDING:



Christy E Ruggiero

Los Alamos National Laboratory

42 PUBLICATIONS 1,187 CITATIONS

[SEE PROFILE](#)



Christopher J Cramer

University of Minnesota Twin Cities

531 PUBLICATIONS 23,105 CITATIONS

[SEE PROFILE](#)

University of Minnesota Supercomputer Institute Research Report UMSI 93/164

UMSI 93/164 September 1993
**SYNTHESIS AND STRUCTURAL AND
SPECTROSCOPIC CHARACTERIZATION
OF MONONUCLEAR COPPER NITROSYL
COMPLEXES: MODELS FOR NITRIC OXIDE
ADDUCTS OF COPPER PROTEINS AND
COPPER-EXCHANGED ZEOLITES**
Christy E. Ruggiero, Susan M. Carrier,
William E. Antholine, James W. Whittaker,
Christopher J. Cramer, and William B. Tolman

1200 Washington Avenue South □ Minneapolis, Minnesota 55415

Synthesis and Structural and Spectroscopic Characterization of Mononuclear Copper Nitrosyl Complexes: Models for Nitric Oxide Adducts of Copper Proteins and Copper-Exchanged Zeolites.

Christy E. Ruggiero,[†] Susan M. Carrier,[†] William E. Antholine,[‡] James W. Whittaker,[§]
Christopher J. Cramer,[†] and William B. Tolman^{†,*}

*Contribution from the University of Minnesota and the Minnesota Supercomputer Institute,
207 Pleasant St. S.E., Minneapolis, MN 55455, the Medical College of Wisconsin, 8701
Watertown Plank Road, Milwaukee, WI 53226, and Carnegie Mellon University, 4400 Fifth
Avenue, Pittsburgh, PA 15213.*

Abstract: We report the synthesis and characterization of the first examples of well-characterized mononuclear copper nitrosyl complexes, $Tp^{RR'}CuNO$ ($Tp^{RR'} = \text{tris}(3-R, 5-R'\text{-pyrazolyl})\text{hydroborate}$; 1: $R = t\text{-Bu}$, $R' = H$; 2: $R = R' = Ph$). These novel $\{\text{CuNO}\}^{11}$ compounds model a possible intermediate in nitrite reduction by the copper nitrite reductase from *A. cycloclastes* and provide chemical precedent for NO coordination to isolated copper sites in proteins and in zeolites. Compounds 1 and 2 were synthesized by treating the copper(I) complexes $[Tp^{t\text{-Bu}}\text{Cu}]_2$ or $Tp^{RR'}\text{CuL}$ ($R = t\text{-butyl}$, $R' = H$, $L = \text{CH}_3\text{CN}$; $R = R' = Ph$, $L = \text{CH}_3\text{CN}$; $R = R' = Ph$, $L = 3,5\text{-diphenylpyrazole}$) with NO (1 atm) in organic solvent. Manometry measurements showed that NO binding is weak, reversible, and temperature dependent, with only 38 (3)% of the available copper in solutions of $[Tp^{t\text{-Bu}}\text{Cu}]_2$ bound to NO at 23 °C. Irreversible displacement of the nitrosyl ligand was effected by addition of excess CH_3CN or CO to yield the respective Cu(I) adducts. Reaction of 1 with O_2 afforded the known complex $Tp^{t\text{-Bu}}\text{Cu}(\text{NO}_3)$. The geometry of 1 was shown by X-ray crystallography to be approximately C_{3v} -distorted

[†] University of Minnesota and the Minnesota Supercomputer Institute

[‡] Medical College of Wisconsin

[§] Carnegie Mellon University

tetrahedral, with bond distances Cu-N = 1.759 (6) Å and N-O = 1.108 (7) Å and bond angle Cu-N-O = 163.4 (6)° (crystal data: monoclinic, space group P2₁/n (#14), at -101 °C, $a = 10.28$ (1) Å, $b = 17.40$ (2) Å, $c = 16.12$ (1) Å, $\beta = 90.0$ (1), $V = 2882$ (8) Å³, $Z = 4$, $R = 0.052$ and $R_w = 0.065$ for 2866 reflections with $I > 3\sigma(I)$ and 293 variable parameters after correction for twinning). Distinctive spectroscopic features of the nitrosyls **1** and **2** include (i) $\nu(^{14}\text{NO}, ^{15}\text{NO}) = 1712, 1679 \text{ cm}^{-1}$ (**1**) and $\nu(^{14}\text{NO}, ^{15}\text{NO}) = 1720, 1687 \text{ cm}^{-1}$ (**2**); (ii) MLCT bands at 494 nm (**1**) and 478 nm (**2**) with $\epsilon \sim 1400 \text{ M}^{-1}\text{cm}^{-1}$; (iii) a lack of MCD features or electronic absorptions above 600 nm; (iv) strong features in their MCD spectra corresponding to the MLCT λ_{\max} values, and (v) EPR spectra with $g_e \sim g_\perp > g_\parallel = 1.83$ and large nitrogen ($A_\perp^{^{14}\text{NO}} = 27 \times 10^{-4} \text{ cm}^{-1}$) and copper hyperfine splitting. These spectroscopic features were shown to contrast with those of the series Tp^{t-BuCuX} (**3**: X = Cl⁻; **4**: X = Br⁻; **5**: X = CF₃SO₃⁻; **6**: X = N₃⁻) that have geometries very similar to that of **1**, but which can be described unambiguously as Cu(II) complexes. Significant spectroscopic features of **3-6** include d → d transitions observable at low energies (> 900 nm) in their electronic absorption and MCD spectra, LMCT bands between 300-600 nm, and rhombic EPR signals with all g values > 2.0 and large copper hyperfine in the high field component consistent with ground states for the complexes having substantial d_{z2} character. The combined evidence from these investigations suggests that the nitrosyl complexes are best described by a molecular orbital picture in which the orbitals with mostly copper d character are fully populated and the unpaired electron resides in a primarily $\pi^*(\text{NO})$ orbital. This qualitative bonding description was supported by all-electron *ab initio* Hartree-Fock and post-Hartree-Fock calculations carried out for a simple analog, the Cu(NH₃)₃NO radical cation, with the heavy atoms constrained to the geometry found from the crystal structure of **1**. Spectroscopic features the synthetic compounds share with purported Cu-NO adducts in both copper proteins and copper-exchanged zeolites are discussed, as is the possible relevance of these compounds to

proposed intermediates in the reduction of nitrite ion by copper-containing nitrite reductase.

Introduction

A critical aspect of the biologically and environmentally significant chemistry of nitric oxide (NO) is its coordination to and activation by transition metal ions.¹ A key intermediate in the interconversions of nitrogen compounds that comprise the global biological nitrogen cycle, NO is produced and consumed via processes mediated by metalloproteins that contain iron or copper. Denitrification, the dissimilatory reduction of oxidized nitrogen-containing compounds (NO_3^- or NO_2^-) to gaseous products (NO, N_2O , and/or N_2) performed by anaerobic bacteria, is an important example of such a process.² The environmental significance of denitrification is profound, in large part because it causes substantial losses of agricultural nitrogen and concomitant production of the greenhouse gas and ozone consumer N_2O .^{2f} Important enzymes involved in denitrification include iron-containing nitrite and nitric oxide reductases, as well as nitrite and nitrous oxide reductases that have copper in their active sites. With the exception of nitrous oxide reductase, metal nitrosyls have been implicated as intermediates in the reactions catalyzed by all of these enzymes,^{3,4} making the MNO unit an important target for structural and mechanistic investigations.

For example, a Cu^+-NO^+ species has been cited as being an intermediate involved in the conversion of nitrite to NO or, in some instances, to N_2O by nitrite reductase from *Achromobacter cycloclastes*,⁴ an enzyme which has been characterized by X-ray crystallography.⁵ Nitrite binding and dehydration to form this nitrosyl (Scheme I) presumably occurs at a single copper site (Cu-II) in the protein which is coordinated to three histidines and a water or hydroxide ligand in a pseudotetrahedral geometry and is linked via a dipeptide segment to a second type 1 copper center (Cu-I) 12.5 Å distant (Figure 1).^{5,6} This type 1 site has been suggested to shuttle electrons to Cu-II via the dipeptide bridge during catalysis.⁷ Largely on the basis of analogies drawn to iron-based systems,^{3a} simple ligand dissociation from the Cu^+-NO^+ unit has been proposed

to provide the principal enzyme product NO and Cu(II), while attack of NO or NO₂⁻ onto the intermediate nitrosyl adduct has been envisioned to yield N₂O (Scheme I).⁴ While examinations of nitrosyls of iron in both protein and synthetic model systems have been - and continue to be - studied extensively,^{8,9} little is known about the chemistry of copper analogs that would shed light on the plausibility of these structural and mechanistic hypotheses.^{10,11}

Several reports of distinct chemical and spectroscopic changes upon treating a wide variety of copper proteins with NO as a structure/function probe provide further impetus for the study of copper nitrosyl complexes, especially since the nature of the copper-NO interactions that are responsible for the observed spectroscopic or redox changes that result from NO treatment remains obscure in most instances.¹² Perhaps the best evidence reported to date for the formation of an adduct between NO and Cu(I) in a protein is the EPR data reported for the product of the reaction of NO with reduced laccase.^{12l} Signals characterized by g values at 2.0 and ~1.8 were observed, as were readily identifiable ¹⁴NO hyperfine splitting in the former component that changed when ¹⁵NO was used. In at least one copper metalloenzyme, NO interactions do not involve the metal center.¹³ Copper nitrosyls have also been identified as possible intermediates in the heterogeneous catalytic decomposition of NO by copper-exchanged zeolites,¹⁴ a process that is attracting attention due to its potential applications in pollution control.¹⁵ Finally, the recent discovery that NO plays a key role in biochemical signal transduction and cytotoxicity has stimulated much research into the associated mechanisms of action,¹⁶ with particular attention being paid toward the role of metal centers in its biological production and reactivity.¹⁷ Although most research to date has been focused on the reactions of NO with iron in heme (guanylate cyclase¹⁸ and NO synthase^{17a-c}) and nonheme¹⁹ environments, the ubiquity of copper proteins suggests the possibility that NO interactions with them also may be important.²⁰

In order to provide fundamental structural and mechanistic information on copper-NO moieties of significance in biological and heterogeneous zeolite environments, we set out to prepare and fully characterize discrete copper nitrosyl model complexes. Such complexes are rare^{10,11} and, until our work, only one compound containing NO bound to copper - a dicopper(II) complex with a bridging NO⁻ ligand - had been structurally characterized.^{11a} Since our initial emphasis has been on modeling the chemistry that occurs at the monomeric catalytic site of nitrite reductase, we have focused our efforts on the synthesis of a mononuclear copper nitrosyl complex containing a coligand that would mimic the tris(imidazolyl) array found at the *A. cycloclastes* protein Cu-II center. The successful synthesis of the first example of such a compound using a sterically hindered tris(pyrazolyl)hydroborate coligand was communicated by us recently.²¹ Here we present details of the synthesis, structural features, and spectroscopic properties of this and related molecules. Spectroscopic data acquired for topologically analogous cupric complexes that contain more 'innocent' ligands than NO will also be presented for comparison to the data acquired for the new nitrosyl compounds. The insight into the electronic structure of the novel copper-NO unit that is provided by consideration of the combined results of structural, spectroscopic, and *ab initio* theoretical studies will be stressed. We will conclude with a discussion of the relevance of the synthetic compounds to analogous species in biological and zeolite-based systems. Portions of this work have appeared in a meeting proceedings.²²

Results

Synthesis and Reactivity. By analogy to the reported synthesis of a Cu(II)-(NO⁻)-Cu(II) complex by treatment of a dicopper(I) compound with NO⁺,^{11a} we initially hypothesized that reaction of a single Cu(I) ion with NO would yield a stable

mononuclear Cu(II)-(NO⁻) species. When purified NO (1 atm) was purged through colorless to pale yellow solutions of [Tp^t-BuCu]₂ or Tp^{RR'}CuL (R = *t*-butyl, R' = H, L = CH₃CN; R = R' = Ph, L = CH₃CN; R = R' = Ph, L = 3,5-diphenylpyrazole)²³ in CH₂Cl₂ or an aromatic solvent (toluene, mesitylene, etc.) at room temperature an almost instantaneous color change to deep red (Tp^t-Bu) or orange (Tp^{Ph2}) was observed (Scheme II). The latter orange solution could also be obtained starting from [Tp^{Ph2}Cu]₂, although the reaction rate was limited by the rate of decomposition of this dimer in solution ($k_{obs} \sim 3.0 \times 10^{-2}$ hr⁻¹ from ¹H NMR spectroscopic monitoring).²³ The colors, which arise from electronic absorption features at 494 nm (Tp^t-Bu) and 478 nm (Tp^{Ph2}), respectively (Figure 2), bleached upon applying a vacuum or by purging with Ar or N₂ and could be restored by retreatment with NO. In the case of the reaction with [Tp^t-BuCu]₂, ¹H NMR analysis of the solution after NO was removed indicated almost complete conversion back to the dimeric cuprous starting material. These observations are consistent with reversible binding of NO to the Cu(I) compounds. Repeated NO/vacuum cycling (>4 times) gradually led to decomposition to unidentified Cu(II) species, indicated by the appearance of a yellow-green color and a broad feature at ~780 nm in the visible absorption spectrum of the NO-depleted solutions. Displacement of NO by addition of excess CH₃CN or CO was also facile, irreversibly affording the Cu(I) adducts Tp^{RR'}CuL (L = CH₃CN or CO; Scheme II). These products were identified by comparison of their ¹H NMR and IR spectra to literature data²⁴ or to data acquired for independently prepared samples.²³

More conclusive evidence of NO coordination to the copper(I) complexes was obtained from infrared spectroscopy. Strong bands at 1712 cm⁻¹ and 1720 cm⁻¹ were observed for the Tp^t-Bu and Tp^{Ph2} adducts, respectively, in NO-saturated solution and in the solid state (*vide infra*). These absorptions were identified as coordinated NO stretching vibrations on the basis of their observed absorptions ~150 cm⁻¹ lower than that of free NO (1875 cm⁻¹) and their shifts to even lower energy upon isotopic

substitution. For $\text{Tp}^{t\text{-Bu}}$ $\nu(\text{NO}) = 1679 \text{ cm}^{-1}$ and for $\text{Tp}^{\text{Ph}2}$ $\nu(\text{NO}) = 1687 \text{ cm}^{-1}$, giving $\Delta\nu_{\text{obs}}(^{14,15}\text{NO}) = 33 (2) \text{ cm}^{-1}$ (observed $\nu^{14}\text{NO}/\nu^{15}\text{NO} = 1.02$) for both in close agreement with the predicted value of $\Delta\nu_{\text{calc}}(^{14,15}\text{NO}) = 31 \text{ cm}^{-1}$ (calculated $\nu^{14}\text{NO}/\nu^{15}\text{NO} = 1.019$). The higher $\nu(\text{NO})$ for the $\text{Tp}^{\text{Ph}2}$ species compared to that for the $\text{Tp}^{t\text{-Bu}}$ case implies that the copper ion in the former is more electron deficient and that the 3,5-diphenyl substituents are slightly electron withdrawing relative to the 3-*t*-butyl groups. A similar trend was observed for the carbonyl stretching frequencies for the corresponding complexes $\text{Tp}^{\text{RR}'\text{CuCO}}$ [$\nu(\text{CO})$ for $\text{Tp}^{t\text{-Bu}} = 2069 \text{ cm}^{-1}$ and $\nu(\text{CO})$ for $\text{Tp}^{\text{Ph}2} = 2086 \text{ cm}^{-1}$].^{23,24}

Manometry experiments showed that NO uptake was incomplete under 1 atm of gas, with NO binding to only 38 (3) % of the available copper ions at room temperature when $[\text{Tp}^{t\text{-Bu}}\text{Cu}]_2$ (in toluene) was used as the starting material. An increase in the amount of NO coordination and a similar increase in absorptivity at 494 nm was observed as the temperature was lowered. These data showed that the copper(I) complex, NO, and the product nitrosyl species were in dynamic equilibrium in solution. By using a literature value for the solubility of NO in toluene,²⁵ an approximate K_{eq} value at 296 K was calculated: $K_{\text{eq}} = [\text{Tp}^{t\text{-Bu}}\text{CuNO}]^2 / [[\text{Tp}^{t\text{-Bu}}\text{Cu}]_2][\text{NO}]^2 = 140 (10) \text{ M}^{-1}$ for 1 atm NO where $[\text{NO}] = 1.11 \times 10^{-2} \text{ M}$ and $[[\text{Tp}^{t\text{-Bu}}\text{Cu}]_2] = 7.2 \times 10^{-3} \text{ M}$. The molar extinction coefficient (ϵ) per copper for the 494 nm absorption band of the $\text{Tp}^{t\text{-Bu}}$ nitrosyl product was determined from the combined gas uptake (concentration of copper nitrosyl) and electronic absorption data. The calculated value of $\epsilon/\text{CuNO} = 1400 \text{ M}^{-1}\text{cm}^{-1}$ is consistent with assignment of the 494 nm band as a charge transfer (CT) transition (*vide infra*). Similar experiments and data analysis for solutions prepared from $\text{Tp}^{\text{Ph}2}\text{Cu}(3,5\text{-diphenylpyrazole})$ yielded the same ϵ/CuNO value within experimental error for the 478 nm absorption feature of the $\text{Tp}^{\text{Ph}2}$ nitrosyl species.

The NO-saturated solutions of the copper(I) starting materials were exceedingly sensitive to dioxygen, in the case of $\text{Tp}^{t\text{-Bu}}$ affording bright green solutions of the

known²⁶ cupric complex $\text{Tp}^t\text{-BuCu}(\text{NO}_3)$ upon exposure to air (Scheme II). The production of the nitrate compound was verified by comparison of EPR, UV-Vis, and FTIR spectra of the green solutions and/or derived crystalline compound with literature data²⁶ and with data obtained from independently synthesized material.²⁷ If the amount of free NO was minimized by evacuating the head space above a frozen NO-saturated solution prior to admission of excess dioxygen, formation of $\text{Tp}^t\text{-BuCu}(\text{NO}_2)$ ²⁸ was observed by EPR and UV-Vis spectroscopy. The unusual rhombic EPR signal of this nitrite complex was particularly diagnostic of its presence. Although additional experiments are needed to elucidate its mechanism of formation, our observations are consistent with initial generation of $\text{Tp}^t\text{-BuCu}(\text{NO}_2)$ that is subsequently oxidized by NO_2 (formed from $\text{NO} + \text{O}_2$) to yield $\text{Tp}^t\text{-BuCu}(\text{NO}_3)$. In fact, treatment of a solution of independently prepared nitrite complex with an air/NO mixture resulted in the formation of the nitrate compound (EPR and UV-Vis spectroscopy).

The nitrosyl adducts $\text{Tp}^t\text{-BuCuNO}$, **1**, and $\text{Tp}^{\text{Ph}2}\text{CuNO}$, **2**, could be obtained as crystalline solids by cooling concentrated NO-saturated solutions of $[\text{Tp}^t\text{-BuCu}]_2$ or $\text{Tp}^{\text{Ph}2}\text{Cu}(3,5\text{-diphenylpyrazole})$, respectively, to -20 °C. Both sets of crystals readily lost NO upon exposure to a vacuum or upon brief drying with an inert gas stream, thus preventing acquisition of elemental analytical data. Interestingly, crystals that had been exposed to vacuum for a period sufficient to decolorize them completely turned red/orange again when placed under a positive pressure of NO at -20 °C, although crystallinity was not maintained due to solvent loss during the process. Upon redissolving the crystals of **1** or **2** in CH_2Cl_2 or aromatic solvent rapid decolorisation and NO loss (identified by GC analysis) was observed, but if gas headspace above a sealed flask was minimized red or orange solutions were generated that exhibited spectroscopic properties identical to those of the NO-saturated solutions of the cuprous starting materials.

X-ray Crystal Structure of $1 \cdot 0.5 \text{ C}_9\text{H}_{12}$. X-ray quality crystals of $1 \cdot nS$ ($S =$ toluene, $n = 1$; $S =$ mesitylene, $n = 0.5$) were mounted by coating them with heavy weight oil and quickly placing them under a cold N_2 stream to inhibit solvate and NO loss. Initial data sets collected with crystals obtained from toluene and chlorobenzene solutions verified the essential connectivity of the complex and the presence of solvate molecules, but extreme disorder of the latter prevented satisfactory refinement of the structures and led to unreasonably large thermal parameters for the critical nitrosyl moiety.²⁹ The degree of solvate disorder was minimized when mesitylene was used as crystallization solvent, but twinning estimated to be 10-15% led to a rather poor initial refinement. By using calculated structure factors that included contributions from the twinned elements (see Experimental Section) satisfactory refinement was finally obtained.

ORTEP drawings of the whole molecule of **1** and its core with significant bond lengths and angles noted are shown in Figure 3. It is apparent that the starting cuprous dimer was cleaved to form the first example of a mononuclear copper nitrosyl complex. The copper coordination geometry is distorted tetrahedral, the local symmetry being close to C_{3v} with the three-fold axis approximately along the Cu-NO bond (N1 lies 0.08 Å from the normal of the plane defined by the N_{pz} atoms). There is relatively symmetrical pyramidal coordination of the Tp^{t-Bu} ligand that is indicated by the similar Cu-N_{pz} bond lengths [range 2.044 (5) to 2.091 (5) Å; avg. 2.063 Å] and N_{pz}-Cu-N_{pz} angles [range 92.7 (2)° to 93.4 (2)°; avg. 93.0°]. Enlarged N1-Cu-N_{pz} bond angles are indicative of the C_{3v} distortion from tetrahedral geometry (range 120.4 (2)° to 124.6 (2)°; avg. 123.1°). Similar bond distances and angles have been observed in pseudotetrahedral complexes of sterically hindered Tp^{RR'} ligands that contain either bona fide Cu(I)^{23,24} or Cu(II)^{26,30} ions, making it difficult to evaluate the electronic structure of **1** on the basis of its metal/Tp^{t-Bu} ligand bonding parameters.

As is typical for transition metal nitrosyl complexes,³¹ the copper nitrosyl unit in **1** is characterized by short Cu-N and N-O bond lengths [1.759 (6) Å and 1.108 (7) Å, respectively]. The latter distance is slightly shorter than the average value of 1.159 Å cited for a wide range of complexes.^{31a} The short Cu-NO distance, like most other M-NO distances, indicates substantial multiple bond character between the copper ion and the nitrosyl ligand. The Cu-N-O angle is 163.4 (6) $^{\circ}$, a slight bending that is intermediate between the usual 180 $^{\circ}$ linear and 120 $^{\circ}$ "bent" metal nitrosyl extremes. Although electronic effects usually predominate among the factors that induce nitrosyl bending (see Discussion),^{1,31b} the possibility that there are steric influences on the Cu-N-O angle in **1** is suggested by the observed orientation of the nitrosyl oxygen atom pointed away from one of the *t*-butyl groups (C26) and toward the space between the other two pyrazolyl substituents.

Electron Paramagnetic Resonance Spectroscopy. The interaction of NO, which has one unpaired electron, and a d¹⁰ Cu(I) ion affords an $S = 1/2$ ground state that should give rise to an EPR signal. Surprisingly, frozen glasses of **1** or **2** in 1:1 CH₂Cl₂/toluene were EPR silent at 77 K, a temperature at which EPR spectra of most Cu(II) complexes are readily recorded.³² We hypothesized that either (i) a facile relaxation mechanism was operative in the complexes that prohibited observation of an EPR signal, or (ii) the complexes dimerized in solution to yield antiferromagnetically coupled species with $S = 0$ ground states that were EPR silent. The latter possibility was deemed unlikely on the basis of the near identity of solution and solid state v(NO) values in the FTIR spectra of the complexes and the eventual observation of EPR spectra at temperatures below 40 K.³³ In Figure 4 are shown X (9.41 GHz)- and S (3.46 GHz)-band EPR spectra, first harmonics, and our current simulations for frozen glasses of Tp^{*t*}-BuCu¹⁴NO (**1**-¹⁴NO) and Tp^{*t*}-BuCu¹⁵NO (**1**-¹⁵NO) at ~30 K. Almost identical spectra for Tp^{Ph}₂Cu¹⁴NO (**2**-¹⁴NO), and Tp^{Ph}₂Cu¹⁵NO (**2**-¹⁵NO) were recorded (data not shown), supporting similar structures for **1** and **2**. Integration of the signals indicated that they

correspond to ~70% of the available copper, consistent with the manometry experiments which showed that nitrosyl formation is not complete under 1 atm NO. Table I lists g and A values that were obtained by simulations in which a common set of parameters were used. The presence of hyperfine coupling to both copper and nitrogen clearly indicates that the signals arise from the copper nitrosyl complexes. The calculation of a consistent set of g and A values for spectra obtained at different frequencies and with ^{14}NO and ^{15}NO ligands suggests that these values are essentially correct, although the ratio $A_{\perp}^{^{15}\text{NO}}/A_{\perp}^{^{14}\text{NO}} = 1.37$ is slightly smaller than the expected theoretical value (1.43; calculated from the ratio of nitrogen nuclear magnetic moments), reflecting some imperfections in our current simulations.

There are several noteworthy features of these spectra that must be rationalized by any bonding model proposed for the copper nitrosyl compounds. First and foremost, a g value significantly less than the free electron value (2.0023) is observed ($g_{\perp} > g_{\parallel} = 1.84$). Copper(II) complexes generally exhibit $g > 2.0$ as a result of the sign of the many-electron spin orbit coupling constant for the d⁹ Cu(II) ion ($\lambda \sim -830 \text{ cm}^{-1}$).^{32,34} The observed low g value thus clearly indicates that a straightforward Cu(II)-(NO⁻) formulation for the complexes is incorrect. A second distinctive feature of the EPR spectra is the large $A_{\perp}^{^{14}\text{NO}}$ value of $27 \times 10^{-4} \text{ cm}^{-1}$ (30 G) which implies that substantial unpaired spin density resides on the nitrosyl nitrogen. For comparison, reported values of ^{14}N hyperfine splitting constants in the direction perpendicular to the bond for the radicals NO³⁵ and N₂³⁶ in matrices or adsorbed onto surfaces are between 20×10^{-4} and $30 \times 10^{-4} \text{ cm}^{-1}$ (Table I). Hyperfine couplings to nitrogen donor atoms in ligands coordinated to Cu(II) complexes are usually smaller ($< 14 \times 10^{-4} \text{ cm}^{-1}$).³² Interestingly, similar low g and high A^{NO} values have been reported for reduced Cu-exchanged zeolites that had been treated with NO (Table I),¹⁴ suggesting that 1 and 2 may model species formed in these heterogeneous systems. Finally, we note that in 1 and 2 the

largest A_{Cu} ($107 \times 10^{-4} \text{ cm}^{-1}$ in **1**) appears in the g_{\parallel} feature that is most perturbed from the free electron value, but A_{NO} is resolved only in g_{\perp} .

The combination of these EPR properties and the facile relaxation process(es) responsible for the non-Curie temperature dependence of the signals point to a unique electronic structural description for the nitrosyl complexes that differs significantly from that expected for a simple Cu(II) compound. To more thoroughly provide support for this conclusion, we have examined the EPR spectra of the series of molecules $Tp^{t\text{-}Bu}CuX$ (**3**: $X = Cl^-$; **4**: $X = Br^-$; **5**: $X = CF_3SO_3^-$; **6**: $X = N_3^-$) that have geometries very similar to that of **1**, but which can be described unambiguously as Cu(II) complexes.^{26,28} The X-ray crystal structures of **3**,^{26b} **5**,²⁸ and a close analog of **6**, $Tp^{i\text{-}Pr}_2CuN_3$,³⁷ have been performed, and we surmise on the basis of comparisons of their spectroscopic properties that **4** and **6** have similar structures to **3** and $Tp^{i\text{-}Pr}_2CuN_3$, respectively. All of the compounds have approximate C_{3v} geometries, with a tridentate Tp and the ligand X in the fourth coordination position just as in **1** and **2**. X-band EPR spectra recorded for frozen glasses of **3-6** at 77 K are shown in Figure 5, and g and A values calculated from spectral simulations are listed in Table II. The spectra exhibit substantial rhombic splitting (Δg_{xy} and Δg_{yz} are ~ 0.2), a g_z value barely perturbed from the free electron value, and the largest copper hyperfine splitting in the highest field (g_z) component. These features are quite distinct from the axial spectra characteristic of tetragonal Cu(II) complexes with $d_{x^2-y^2}$ ground states and are instead consistent with ground states having substantial d_{z^2} character.^{32,34} Qualitatively similar spectra have been measured for the distorted tetrahedral sites in stellacyanin,³⁸ cucumber basic blue protein,³⁹ and Cu(II)-substituted insulin hexamer containing exogenous thiolate,⁴⁰ although the spectra of **3-6** are characterized by much larger rhombic splitting and greater g_x and g_y values (Table II). Most importantly for the purposes of this discussion, the observation of g values greater than 2.0 combined with the generally different appearance of the

signals for **3-6** compared to those of the nitrosyls **1** and **2** argue for distinct electronic structural descriptions for the two sets of compounds.

Electronic Absorption and Magnetic Circular Dichroism Spectroscopy. As indicated in Figure 6, the longest wavelength (lowest energy) features in the ambient temperature absorption and 4 K MCD spectra of solutions of **1** and **2** lie below 600 nm (Near-IR absorption spectral data for **2** not shown is also featureless). The absence of absorption and MCD features to longer wavelengths is a distinctive aspect of the spectroscopic properties of the nitrosyl compounds that contrasts with the data obtained for the Cu(II) complexes **3-6**. As shown in Table III and exemplified by the spectra shown in Figure 7 for **3**, absorption bands and MCD intensity which we assign to ligand field transitions are observed for the Cu(II) complexes well into the near-IR region. These bands appear at particularly long wavelength compared to those usually observed for tetragonal, square pyramidal, or even D_{2d} -distorted (pseudotetrahedral) Cu(II) compounds.⁴¹ The relatively small ligand field splitting and corresponding low energy $d \rightarrow d$ absorption bands in **3-6** are characteristic of the low coordination number and near-tetrahedral symmetry. These Cu(II) compounds also exhibit charge transfer bands in the visible region of their absorption spectra and corresponding MCD features (Table III). As anticipated for LMCT transitions, these absorptions are shifted to longer wavelength in the bromide complex **4** compared to the chloride **3** as a result of the differences in ligand field strengths of the halides.⁴² However, we have not yet carried out extensive investigations that would allow definitive assignment of the LMCT features in **3-6**, which could arise from pyrazole $\pi \rightarrow \text{Cu(II)} d$ or $X \pi \rightarrow \text{Cu(II)} d$ transitions.^{42,43}

In contrast to these bona fide Cu(II) complexes, the absorption features at 494 nm and 478 nm for **1** and **2**, respectively, have relative energies that are most consistent with their assignment as MLCT transitions (they shift to higher energy as the electron density at the metal center decreases).⁴² For **1**, two transitions are partly resolved in

absorption with approximately 5000 cm^{-1} splitting. At low temperature in an applied magnetic field, MCD intensity is induced in these absorption bands with a pattern of nearly equal and opposite intensity characteristic of an MCD intensity mechanism involving spin orbit coupling over excited states.⁴⁴ This is consistent with a description of the excited state as Cu(II)-(NO⁻) (spin paired on NO) with the spectral splitting corresponding to the tetrahedral ligand field splitting in the Cu(II) final state. Again, profound differences between the absorption and MCD spectroscopic properties exhibited by the nitrosyls **1** and **2** compared to the Cu(II) species **3-6** corroborate their divergent electronic structures.

Theoretical Calculations of Electronic Structure. In order to gain further insight into the electronic structure of **1**, all-electron *ab initio* Hartree-Fock (HF) and post-Hartree-Fock calculations were carried out for a simple analog, the Cu(NH₃)₃NO radical cation. The heavy atoms were constrained to the geometry found from the crystal structure of **1**, while the ammonia hydrogen atoms were arbitrarily assigned to ideal positions. Under these conditions, unrestricted Hartree-Fock calculations predict the ground state electronic wavefunction to be of $^2\text{A}'$ symmetry, i.e. the unpaired electron is in the symmetry plane of the molecule (Figure 8). However, the *relaxed* orthogonal $^2\text{A}''$ state lies a mere 0.9 kcal mol⁻¹ higher in energy. Moreover, as predicted by more qualitative molecular orbital arguments (*vide infra*), the corresponding SOMO's for these two states are primarily the nitrosyl π^* MO's with $\pi_{\text{Cu}-\text{N}}$ antibonding contributions from appropriate copper orbitals (i.e., the SOMO and LUMO in Figure 8). The extent of the contributions of the copper and nitrosyl atomic wave functions to the $26\text{a}'$ molecular orbital wave function (SOMO) are 27% and 54%, respectively, with the remaining contributions coming from the NH₃ ligands as graphically illustrated in Figure 8. It is also noteworthy that the analogous contributions to the $11\text{a}''$ orbital, which would be singly populated in a low-lying excited state of the molecule, are 51% (Cu) and 3% (NO).

The presence of very low lying virtual orbitals suggests that the Hartree Fock microstate is probably a poor representation of the molecular wavefunction. Configuration interaction calculations including all single and double excitations (CISD) support this assessment, with the coefficient of the $^2A'$ HF wavefunction indicating only 83% contribution to the CISD wavefunction. As a result, still more sophisticated treatments would be desirable to accurately model the electronic structure of 1. However, the CISD results represent a practical limit given the size of this system.

From the HF and CISD spin densities, we may calculate EPR isotropic hyperfine couplings to the magnetic nuclei. Inclusion of correlation changes the sign of the ^{15}N hyperfine coupling, although interestingly the magnitude is similar in both the HF ($24 \times 10^{-4} \text{ cm}^{-1}$) and CISD ($-20 \times 10^{-4} \text{ cm}^{-1}$) cases. Given the better quality of the CI wavefunction, we assume the experimental tensor components to be negative (sign is not determined under these conditions). The agreement with the observed ^{15}N isotropic hyperfine couplings ($-24 \times 10^{-4} \text{ cm}^{-1}$, assuming A_{\parallel} to be very close to zero since it is not observed spectroscopically) is well within experimental error. However, at neither the HF nor the CISD levels is the agreement between theory and experiment even qualitative for ^{63}Cu , where the predicted hyperfine couplings are less than $1 \times 10^{-4} \text{ cm}^{-1}$. This is disappointing, but not altogether unexpected, since it is extremely difficult to accurately model the spin polarization of the core s orbitals which, by virtue of their large magnitude at the nucleus, may contribute significantly to the observed hyperfine coupling even though they play no appreciable role in the SOMO.⁴⁵ What is evident from the calculations, however, is that there is apparently little tendency for net spin to reside on copper by virtue of a metal to ligand electron transfer to form Cu(II) in the ground state.

A configuration interaction analysis of single electronic excitations (CIS)⁴⁶ is consistent with the view that, with all d orbitals filled, no LMCT excitations are observed. Thus, the first transition is predicted to occur in the near IR (3800 nm,

oscillator strength $f < 10^{-4}$) for the symmetry-forbidden⁴⁷ $26a' \pi^* \rightarrow 12a'' \pi^*$ excitation on the nitrosyl (i.e. no metal electrons are involved). Transition 2 is a weak ($f = 0.0010$) allowed transition at 241 nm dominated by $11a'' d_{yz} \rightarrow 12a'' \pi^*$ (taking the CuNO symmetry plane as xz , Figure 8), with the α and β components of the excitation vector out of phase. Transitions 3 and 4 are overlapping forbidden transitions ($f = 0.0010$ and $f=0.0009$) at 212 and 209 nm corresponding to $24a' \rightarrow 12a'' \pi^*$ and $25a' \rightarrow 12a'' \pi^*$ respectively, where the two a' orbitals are opposite linear combinants of the copper d_{z^2} and $d_{x^2-y^2}$ orbitals. Finally, transition 5 is a strong, allowed transition ($f = 0.0249$) at 189 nm which also corresponds primarily to $11a'' d_{yz} \rightarrow 12a'' \pi^*$, now with the α and β components in phase. This agrees qualitatively with the results presented in Table III. Given the great simplification of the Tp ligand in the theoretical model,⁴⁸ and the lack of diffuse functions in the basis set for the CIS calculations,⁴⁶ it is not surprising that the calculated transition energies are higher than those observed experimentally; the important point is that the lowest energy allowed transitions are predicted to be MLCT transitions involving predominantly $Cu(d) \rightarrow NO(\pi^*)$ excitations.

Finally, a simple Mulliken analysis places a partial atomic charge of only +0.55 electronic charge units on copper, with the nitrosyl having a net charge of +0.06 and the remainder distributed over the three ammonia groups. Thus, there is no indication that the compound should be viewed as having an ionic $Cu(II)-(NO^-)$ interaction. Rather, theory appears to support in every instance assignment of **1** as a highly covalent nitrosyl species (*vide infra*).

Discussion

Structure and Bonding. According to the formalism introduced by Feltham and Enemark,^{31a} the complexes **1** and **2** have $\{CuNO\}^{11}$ electron configurations; i.e., the total number of electrons associated with the metal d orbitals and the NO π^* orbitals is 11. To

our knowledge, the highest electron counts reported are $\{\text{MNO}\}^{10}$, making the copper nitrosyls unique. The question of how the 11 electrons in **1** and **2** are distributed has been a major focus of our structural, spectroscopic, and theoretical studies. While the covalency normally associated with metal-nitrosyl bonds makes assigning oxidation states to the metal and to NO a futile undertaking,³¹ as a working hypothesis one can nonetheless view the $\{\text{CuNO}\}^{11}$ unit in terms of limiting valence bond structures $\text{Cu(I)}\text{-}(\text{NO}\cdot)$, $\text{Cu(0)}\text{-}(\text{NO}^+)$, or $\text{Cu(II)}\text{-}(\text{NO}^-)$. The former formulation indicates adduct formation between the starting Cu(I) ion and NO with limited charge transfer in the ground state, while the latter two imply electron transfer either to or from the metal ion, respectively. In view of the nature of the N-donor environment provided by the $\text{Tp}^{\text{RR}'}$ ligands, the rarity of isolable Cu(0) coordination compounds, and the oxidizing power of NO^+ , we view the $\text{Cu(0)}\text{-}(\text{NO}^+)$ picture as the least satisfactory way to describe the complexes and we will not consider it further. Precedent for the $\text{Cu(II)}\text{-}(\text{NO}^-)$ description can be found in the only other known copper nitrosyl complex to be isolated, $[\text{Cu}_2(\text{XYL-O}^-)(\text{NO})](\text{PF}_6)_2$.^{11a} It was assigned as a $\text{Cu(II)}\text{-}(\text{NO}^-)\text{-Cu(II)}$ species on the basis of observed low $\nu(\text{NO})$ (1536 cm^{-1}), dd bands in its electronic absorption spectrum, and a 5-coordinate square pyramidal copper ion geometry in its X-ray crystal structure.^{11a} Electron transfer to NO has also been postulated for $\{\text{FeNO}\}^7$ species formed from Fe(II) and NO, a most recent example being the $\text{Fe(III)}\text{-}(\text{NO}^-)$ ground state formulation proposed on the basis of extensive spectroscopic studies for nonheme nitrosyls in soybean lipoxygenase and some model complexes.^{9a}

The combined results of the structural, spectroscopic, and theoretical work described herein favor the $\text{Cu(I)}\text{-}(\text{NO}\cdot)$ description over the $\text{Cu(II)}\text{-}(\text{NO}^-)$ formulation for **1** and **2**, however. Alternatively, a qualitative molecular orbital picture can be used to describe the bonding that more explicitly accounts for the covalency intrinsic to the CuNO unit and that better allows the observed spectroscopic properties of the complexes to be rationalized (Figure 9). This molecular orbital energy level diagram is

identical to that previously^{31b} derived via qualitative ligand field theory arguments for known tetrahedral {MNO}¹⁰ complexes that contain three equivalent ligands,⁴⁹ the local C_{3v} symmetry of these compounds being closely analogous to that observed for **1**. In the 10-electron systems, all the metal orbitals are filled except for the degenerate 4e set, which is comprised of antibonding combinations of the d_{xz} and d_{yz} orbitals with the π* NO orbitals of the same symmetry. The observed linearity of the metal nitrosyl in these {MNO}¹⁰ complexes is nicely rationalized by the vacancy in the 4e set.^{31b} Using this MO scheme as a starting point, one predicts that the added electron in a {CuNO}¹¹ overall configuration will be Jahn-Teller active, resulting in a geometric distortion that lifts the 4e orbital degeneracy. The partially filled 4e orbital is antibonding between the metal and the ligand [π*(NO)-d_{xz,yz}], and population of this orbital leads to bending of the nitrosyl. Indeed, bending of the Cu-NO unit is observed in the X-ray structure of **1**, but its extent is relatively small (~17°), consistent with only partial occupation of the antibonding levels. The observed ν(NO) of 1712 cm⁻¹ (**1**) sheds limited light on the CuNO bending since it is in the region (1600-1800 cm⁻¹) where nitrosyl stretches in linear and bent complexes overlap.^{31c}

More sophisticated *ab initio* calculations that we have performed on the model complex Cu(NH₃)₃NO corroborate the above qualitative assessment of the nature of the frontier orbitals in the nitrosyl complexes and afford additional insight into the covalency of the Cu-NO interaction. Similar to the MO diagram in Figure 9, the calculations show that the orbitals of predominantly d character are filled and that the SOMO (26a') and LUMO (12a'') have large π*(NO) contributions and lie close in energy (Figure 8). The calculated extent of the copper and nitrosyl contributions to the SOMO (27% and 54%, respectively) indicates the large degree of NO character in this orbital and implies substantial covalency in the CuNO interaction. The exact ordering of the metal d orbitals and the nature of the d(Cu)/π*(NO) interactions shown in Figure 9 differ from those predicted using the qualitative MO picture (Figure 8), however, partly

because of extensive mixing within the d orbital manifold. This mixing, the lack of charge separation calculated from the Mulliken analysis, and the relative contributions of the copper and nitrosyl atomic wave functions to the overall molecular orbital wave function for the SOMO are direct reflections of the covalency of the system.

The EPR, electronic absorption, and MCD results obtained for **1** and **2** can be successfully interpreted, at least in a qualitative fashion, by reference to either the simplified MO picture (Figure 9) or the frontier orbitals calculated by *ab initio* methods (Figure 8). Turning first to the EPR data, the substantial differences between the spectra of **1** and **2** (Figure 4) compared to those of **3-6** (Figure 5), especially with respect to g values and temperature dependencies, argue against a straightforward Cu(II) formulation for the nitrosyls. The observation of $g_e \sim g_{\perp} > g_{\parallel} = 1.84$ for **1** is particularly striking, since g values for Cu(II) ions are expected to be greater than the free electron value as a consequence of the greater-than half-filled (d^9) shell.³² A similar pattern of g values to that observed for the nitrosyl complexes is found in EPR spectra of the diatomic radicals N₂⁻ and NO trapped in matrices or adsorbed onto surfaces.^{13,35,36} These spectra are characteristic of low symmetry perturbed $^2\Pi$ ground states for these radicals. Both species have a (π^*)¹ valence electron configuration and both exhibit g-shifts below the free electron g-value (2.00), the sign of the g-shifts being a direct consequence of spin orbit mixing within the less-than half-filled valence shell and the magnitude of the g-shift being inversely proportional to the splitting of the π^* orbitals. Any low symmetry distortion that lifts the π^* orbital degeneracy will quench the effective L = 1 orbital angular momentum for a Π state, but spin orbit mixing within this near-lying doublet pair of states unquenches the L_z = 1 component of orbital momentum. This simple picture is substantiated by detailed calculations of spin orbit interactions for NO in low symmetry.³⁵ The NO bond defines the molecular z-axis along which the orbital momentum is unquenched, so the largest g-shift is expected to be associated with g_z (see g_{||} values listed in Table I). Experimentally, the largest ¹⁴N

hyperfine coupling for NO and N₂⁻ is observed in the perpendicular g-values (see A_⊥ values in Table I).

This is also true of **1** and **2**, where similar magnitudes of A_⊥¹⁴NO are observed, with relatively small nitrogen hyperfine splittings in g_{||}. The large value of A_⊥^N in these molecules is a consequence of the unpaired spin density in a component of the 4e MO in Figure 9 (or the 26a' orbital shown in Figure 8) having significant π*(NO) character, for which dipolar contributions to the electron nuclear hyperfine coupling will maximize for the magnetic field in the molecular xy-plane. The close agreement of the nitrosyl nitrogen hyperfine coupling calculated from HF and CISD spin densities with that observed experimentally supports this overall description. Other "electron excess" metal complexes with their SOMO localized on ligands are known, the 19 electron species M(CO)₂(NO)₂ⁿ⁻ (M = Fe, n = 1; M = Co, n = 0) being particularly relevant because, like **1** and **2**, they have been described as having essentially d¹⁰ metals and a SOMO with significant π*(NO) character that gives rise to EPR spectra with g < 2.0 and large ¹⁴N hyperfine.⁵⁰

The analogies between the EPR parameters of **1** and **2** and those for NO and N₂⁻ trapped in matrices or adsorbed on surfaces thus suggest that the perturbation of NO upon binding to Cu(I) in the complexes is minor. In fact, it is important to note that observation of copper hyperfine in g_{||} is a critical indication that the spectra arise from a CuNO unit, and not merely from NO trapped in the frozen solvent matrix.⁵¹ On the other hand, the presence of significant unpaired spin density at the copper nucleus is implied by the magnitude of A_{||}^{Cu} (107 x 10⁻⁴ cm⁻¹). This observation, in combination with the short Cu-NO bond, is consistent with the covalency and multiple bond character in the copper nitrosyl bond that is implied by the Mulliken charge distribution and the substantial contribution of copper atomic orbitals (27%) to the SOMO calculated for the model system.

The electronic absorption and MCD data for **1** and **2** can also be understood by referring to the qualitative MO diagram or the *ab initio* calculations. As predicted by these bonding models, in which all of the orbitals that are principally d in character are filled, no features due to d → d transitions appear in the visible or near-IR regions of the absorption and MCD spectra (Figure 6). This is in marked contrast to the spectra exhibited by the Cu(II) complexes **3-6** which contain quite distinct d → d features (Figure 7). The lowest energy allowed electron transition in the nitrosyls is the band just below 500 nm. Due to the fact that it is shifted to higher energy in **2**, which on the basis of its higher v(NO) has a more electron deficient copper ion, we assign this band as a MLCT transition.⁴² Such transitions are common in Cu(I) complexes of ligands with vacant and low energy π orbital systems such as bipyridines.⁵² Excitation into vacant pyrazole-based orbitals in the nitrosyl complexes would appear unlikely based on the lack of analogous CT bands between 300-500 nm in other TpCu(I) complexes.^{23,24} We therefore favor assignment of this transition in **1** and **2** to a Cu(I) (d) → NO (π*) type MLCT resulting in an excited state of predominantly Cu(II)-(NO⁻) character. This assignment is corroborated by our configuration interaction analysis of single electronic excitations in the Cu(NH₃)₃NO model, in which no LMCT transitions were found. Attribution of cupric character to the excited state is supported by the calculated copper (51%) and nitrosyl (3%) atomic orbital contributions to the 11a^{''} orbital (the origin of the lowest energy allowed excitation). The pseudo A-term in the MCD spectra associated with the partially resolved components of the MLCT transition is also consistent with this assignment. The large spin orbit coupling and small orbital splittings expected for a nearly tetrahedral cupric ion in the final state qualitatively account for the observed pattern of MCD intensity.⁵³ Efforts to definitively assign the MLCT band by measuring the resonance Raman excitation profile for the v(NO) of **1** are in progress, although difficulties associated with apparent photoinduced loss of NO from the complex are hampering our efforts.

In sum, all the evidence acquired to date supports a molecular orbital description for the bonding of NO to the $\text{Tp}^{\text{RR}'}\text{Cu}$ fragment in which the SOMO is principally NO π^* in character and the orbitals based mostly on copper are filled. This result contrasts with the situations observed for the $\mu\text{-(NO⁻)}$ -dicopper(II) complex prepared by Karlin and coworkers^{11a} and the nonheme Fe(III)-(NO⁻) species examined by Solomon et al.^{9a} The relatively decreased tendency of Cu(I) to oxidize to Cu(II) in **1** and **2** is reflected by the $E_{1/2}$ values measured by cyclic voltammetry for the redox couples $\text{Tp}^{\text{RR}'}\text{Cu(I)L}/\text{Tp}^{\text{RR}'}\text{Cu(II)L}^+$, where, for example, $E_{1/2} = +0.93$ V vs. SCE for R = *t*-Bu, R' = H, and L = CH₃CN (0.1 M TBAOTF in 10% CH₃CN/CH₂Cl₂) and $E_{1/2} = +0.69$ V vs. SCE for R = R' = Ph and L = 3,5-diphenylpyrazole (0.1 M TBAH in CH₂Cl₂).²³ As discussed in more detail elsewhere,²³ these redox potentials are anomalously high for copper complexes of nitrogen donor ligands, and presumably result from thermodynamic stabilization of the Cu(I) and destabilization of the Cu(II) states caused by enforcement of a pseudotetrahedral geometry by the sterically hindered $\text{Tp}^{\text{RR}'}$ ligands. This argument also helps rationalize the lack of Cu(II)-(NO⁻) character in the ground states of **1** and **2**. Moreover, according to this model, Cu(I) complexes with lower $E_{1/2}$ values would be predicted to be better able to transfer an electron to NO upon binding and thus would be expected to exhibit significantly different spectroscopic properties from those observed for **1** and **2**, an hypothesis which we are currently attempting to test.

Relevance to Biology and Heterogeneous Catalysis. As the first structurally characterized examples of mononuclear copper nitrosyl complexes, compounds **1** and **2** represent important speculative and replicative models for active site NO adducts to isolated copper ions in biological and heterogeneous environments. First, they model a possible intermediate in nitrite reduction by copper enzymes, in particular nitrite reductase from *A. cycloclastes*. Although it has one more electron than the proposed⁴ protein Cu(I)-(NO⁺) product of dehydration of an initial Cu(I)-(NO₂⁻) species, a

{CuNO}¹¹ unit in the enzyme may be envisioned to form upon one electron reduction of the dehydration product or simply by binding of NO to the reduced active site in a reaction analogous to the synthetic routes to **1** and **2**. The latter possibility, which has been suggested previously,^{11b} is supported by the recent demonstration that incorporation of nitrogen from NO into the enzyme product N₂O is a component of the nitrite reduction pathway.^{4c} Preliminary results from our laboratory have shown that by using a slightly different supporting ligand system (Tp^{Me2}), N₂O generation can be induced from a copper nitrosyl complex analogous to **1** and **2**.²⁹

The copper nitrosyl complexes also model possible adducts between NO and other reduced copper proteins, although unambiguous evidence supporting the existence of such adducts is currently scarce. Studies of the reactions of NO with copper proteins often begin with oxidized copper sites and cite as evidence for NO binding the bleaching of EPR and/or electronic absorption features upon NO treatment and the subsequent restoration of these signals after purging or photolysis.^{12a,p} If such binding occurs in these cases (it is sometimes not clear whether charge-transfer complex formation occurs instead) a {CuNO}¹⁰ configuration different from **1** and **2** would be the result. Reaction of reduced hemocyanin and tyrosinase with NO has been reported to yield N₂O and half-met [Cu(I)-Cu(II)] and, ultimately, met [Cu(II)-Cu(II)] forms of the proteins.^{12c,i,j} Initial formation of a {CuNO}¹¹ species may occur during these transformations, although it has been argued that NO₂ rather than NO is the actual oxidant in the hemocyanin reaction.⁵⁴ In addition, the presence of a second nearby copper ion in these and other multicopper proteins^{12d,m,q} clearly complicates matters by allowing multielectron redox chemistry to ensue. Recent studies of NO interactions with another Cu metalloenzyme, galactose oxidase, suggest that NO may interact at protein sites other than a metal center.¹³ The EPR spectrum of that complex is distinct in that no Cu hyperfine splittings are observed. The observation of signals with g values at 2.0 and ~1.8 and hyperfine splitting to ¹⁴NO and ¹⁵NO in the EPR spectra of NO-treated

reduced laccase represents the clearest evidence to date for adduct formation between NO and Cu(I) in a protein.^{12l} The authors' postulate of a Cu(I)-(NO[·]) adduct based on this data and their argument that the high redox potential of the binding site was responsible for preventing copper oxidation by NO seems reasonable considering our results. In general, however, there remains a great deal of confusion in the literature regarding the often complex chemistry observed in the reactions of NO with copper proteins, and it is our hope that future studies will benefit from the data acquired for synthetic model compounds such as **1** and **2**.

Finally, EPR spectra quite similar to those of **1** and **2** have been observed upon NO treatment of copper-doped ZSM5 zeolites that had been first reduced (so that the metal ions were in the Cu(I) form).^{13a,c,d} Developing an understanding of the NO chemistry of zeolites is important due to their applicability toward catalysis of NO_x decomposition for pollution control.¹⁴ Low g values and substantial A^{NO} were noted in the EPR spectra (Table I) and it was suggested that the adducts giving rise to these signals were best described as Cu(I)-(NO[·]) species. Compounds **1** and **2** provide the first definitive precedent for this proposal. More complex polynitrosyl adducts to one or more copper ions in ZSM5 have also been postulated on the basis of infrared spectroscopic studies.^{13b} The generally higher energy of the v(NO) bands observed in these systems (1730-1970 cm⁻¹) compared to **1** and **2** is consistent with reduced electron density at copper in the oxygen-rich zeolite environment compared to that provided by the sp²-N donor set of the Tp^{RR'} ligands. Like in the model complexes, enforcement of trigonal or tetrahedral copper ion geometries within the zeolites may be responsible for the lack of observed internal charge transfer in the ground state of the adducts in these heterogeneous systems, although more detailed structural information on the topology of the copper-zeolite site(s) that bind NO is needed to corroborate this argument.

Conclusion

The first well-characterized examples of mononuclear copper nitrosyl complexes have been prepared by treating $\text{Tp}^{\text{RR}'}\text{Cu}(\text{I})$ complexes with NO. Manometric, ligand displacement, X-ray crystallographic, and IR, EPR, electronic absorption, and MCD spectral studies were performed which shed substantial light on the reversibility of NO coordination and the geometrical and electronic structural features of these novel $\{\text{CuNO}\}^{11}$ molecules. The combined evidence from these investigations and *ab initio* theoretical work suggests that the nitrosyl complexes are best described by a molecular orbital picture in which the orbitals with mostly copper d character are fully populated and the unpaired electron resides in a primarily $\pi^*(\text{NO})$ orbital. As further support for this assignment, we have also shown that these nitrosyls are spectroscopically distinct from topologically analogous C_{3v} -distorted tetrahedral $\text{Tp}^{\text{RR}'}\text{Cu}(\text{II})\text{X}$ complexes. The title compounds provide key chemical precedent for a possible intermediate in denitrification reactions catalyzed by copper nitrite reductase and for NO adducts to isolated copper sites in other proteins and in copper-exchanged zeolites.

Experimental Section

General Procedures. All reagents and solvents were obtained from commercial sources and used as received unless noted otherwise. Solvents were dried according to published procedures⁵⁵ and distilled under N₂ immediately prior to use. Nitric oxide (NO) gas (Matheson) was purified by passing it through a series of traps (12M NaOH/6M H₂SO₄/drierite/KOH pellets/P₂O₅ mixed with CaSO₄) and then through a dry ice/acetone (196 K) bath according to an adaptation of a literature method.⁵⁶ ¹⁵NO gas (Cambridge Isotopes) was used without further purification. All air-sensitive reactions were performed either in a Vacuum Atmospheres inert-atmosphere glovebox

under a N₂ atmosphere or by using standard Schlenk and vacuum line techniques. Preparative procedures for the complexes [Tp^{RR'}Cu]₂,²³ Tp^{RR'}Cu(CH₃CN),²³ Tp^{Ph2}Cu(3,5-Ph₂pz),²³ and Tp^{t-Bu}Cu(OAc)²⁸ are published elsewhere (R = *t*-butyl, R' = H or R = R' = Ph). Gas chromatography experiments were performed on a Hewlett Packard 5890 series II gas chromatograph with a HP 3396 series II integrator using a Porpak Q column (6 ft., 20 mL/min flow rate, 30 °C, helium carrier gas). Elemental analyses were performed by Atlantic Microlabs of Norcross, GA.

Spectroscopy. IR spectra were recorded on a Perkin Elmer 1600 series FTIR spectrophotometer. Room temperature electronic absorption spectra were recorded on a Hewlett-Packard HP8452 spectrophotometer (200-820nm scan range) interfaced with a microcomputer for data acquisition. Samples were prepared in freshly distilled CH₂Cl₂ and solvent was used as the reference. Absorption spectra were also recorded on Varian Cary 5E or 17D UV-Visible-Near IR spectrometers (300-1800 nm) interfaced with microcomputers for data acquisition. Samples for near-IR absorption spectroscopy were prepared in CDCl₃ or CD₂Cl₂ under argon or N₂. A solvent reference was used for all samples except the nitrosyl complexes, for which solutions of the parent cuprous complex served as a spectroscopic blank.

Low temperature MCD spectra were measured on an AVIV Model 41DS spectropolarimeter equipped with an Oxford Instruments SM4-6T magnetocryostat as described in detail elsewhere.⁵⁷ For near-IR MCD experiments, a liquid N₂-cooled InSb photovoltaic photodiode having a 1 mM square active area was used for signal detection. MCD samples were prepared anaerobically in freshly distilled CH₂Cl₂/toluene glassing solvent. Optical quality glasses were prepared by slowly cooling these samples, and each sample was checked for depolarization by a published method.⁵⁸ The concentration of complex in each sample of 3-6 was determined by copper quantitation with atomic absorption spectroscopy (AAS), while the concentration of 1 and 2 was estimated from the manometry data (38% and 48% NO

bound at ambient temperature, respectively) and the total copper determined from AAS. Aliquot samples were dried and redissolved in hot nitric acid then diluted to approximately 10 ppb Cu with 0.1% nitric acid. Copper analyses were performed on a Varian SpectrAA 20B atomic absorption spectrometer equipped with a GTA-96 graphite furnace.

X-band EPR spectra were recorded either at the University of Minnesota (U.M.) or at the National Biomedical EPR center in Milwaukee (N.B.M.). At U.M., spectra were obtained by using a Bruker ESP300 spectrometer fitted with a liquid nitrogen finger dewar (77 K, ~9.41 GHz) or a Varian E-109 spectrometer with an Oxford instruments liquid helium cryostat (4-50 K, ~9.2 GHz). Temperature and g-value calibrations were performed as previously described.⁵⁹ At the N.B.M. a Bruker ER200D and a Varian Century Series spectrometer were used to record X-band (9.1 GHz) EPR spectra. A gauss meter (Rawson-Lush Instrument Co., Inc., Acton MA) was used to calibrate the magnetic field and a frequency counter (EIP, model 548) was used to determine the microwave frequency. Loop-gap resonators and low-frequency bridges used for measurements at S-band (3-4 GHz) were designed and built at N.B.M.⁶⁰ The temperature was maintained at ~30 K with an Air Products (Allentown, PA) helium flow system. The first harmonic of first derivative spectra was obtained by using SUMSPC92, a data manipulation program available upon request from the N.B.M.⁶¹ All samples were run as 1:1 CH₂Cl₂/toluene frozen glasses. Quantitation of signals were performed using the method of Aasa and Vänngård⁶² with copper sulfate (1.0 mM CuSO₄, 20% glycerol, 2.0 M NaClO₄, 0.1 M HCl) or copper oxalate (1.0 mM CuSO₄, 2.0 mM Na₂C₂O₄, 20% glycerol, 2.0 M NaClO₄, 0.1 M HCl) solutions as integration standards. The programs JDLABS⁶³ and QPOW⁶⁴ were used to simulate experimental spectra. The simulations utilized a spin Hamiltonian of the form given by equation 1,

$$\mathbf{H} = \beta \mathbf{H} \bullet \mathbf{g} \bullet \mathbf{S} + \mathbf{S} \bullet \mathbf{A} \bullet \mathbf{I} \quad (1)$$

where H is the magnetic field vector, S and I are the electron and nuclear spins respectively, \mathbf{g} is the g tensor, \mathbf{A} is the hyperfine tensor, and β is the Bohr magneton. A and g were assumed to have the same principal axes, and a gaussian lineshape was used. The values of the g and A parameters giving the best fit with the experimental data were found by trial and error procedures.

Manometry. Gas uptake experiments were performed by using an apparatus designed similarly to previously reported equipment⁶⁵ which consisted of a mercury manometer connected through a Teflon stopcock to a glass side arm. A standard 25 mL Schlenk flask, used as the reaction vessel, was connected to the side arm with a short piece of tubing. The side arm was connected through a glass "T" to a second Teflon stopcock, then to a 3-way glass stopcock which was linked to both vacuum and gas inlet lines. The powdered sample (cuprous starting material or calibration standard) was stored in a very small flask connected to the Schlenk flask with a ground glass joint, and was initially closed off from the system with a Teflon stopcock. The system, including the Schlenk flask containing the reaction solvent (CH_2Cl_2), was evacuated and refilled with the reacting gas (NO or CO) three times to insure a pure atmosphere in the system. The system was then filled with reacting gas, shut off from the gas/vacuum inlet with the second Teflon stopcock, and the initial pressure was recorded. The powdered sample was then opened and allowed to fall into the solvent in the Schlenk flask whereupon it immediately dissolved. The solution was kept in a constant temperature bath and vigorously stirred with a magnetic stir bar. The pressure change in the system was recorded until it stabilized (1 h). The volume of the system was calibrated by measuring the uptake of CO by $[\text{Tp}^{t\text{-Bu}}\text{Cu}]_2$ under conditions identical to those used for the copper/NO uptake experiments, except due to the absorption of CO by powdered $[\text{Tp}^{t\text{-Bu}}\text{Cu}]_2$ pressure equilibration under Ar was performed prior to the addition of CO. Quantitative formation of $\text{Tp}^{t\text{-Bu}}\text{CuCO}$ was confirmed by ^1H NMR spectroscopy. The moles of gas absorbed was then calculated using the ideal gas law. For example, two

runs with $[Tp^{t\text{-Bu}}\text{Cu}]_2$ [1.93 (1) $\times 10^{-4}$ mol and 1.91 (1) $\times 10^{-4}$ mol] dissolved in 10 mL toluene absorbed 1.47 (8) $\times 10^{-4}$ mol and 1.44 (8) $\times 10^{-4}$ mol NO, respectively, which upon averaging implied NO coordination to 38 (3)% of the available copper ions.

Tp^t-BuCuNO (1). $[Tp^{t\text{-Bu}}\text{Cu}]_2$ (236 mg, 0.265 mmol) was dissolved in ~2 mL aromatic solvent (toluene or mesitylene) in a Schlenk flask. The flask was purged with NO gas with vigorous shaking until the solution turned deep red (< 1 min). Bright red crystals of $1 \cdot nS$ ($S =$ toluene, $n = 1$; $S =$ mesitylene, $n = 0.5$) formed upon allowing the solution to stand for 2-3 days at -20 °C. The crystals were collected by quickly filtering the solution under Ar, and then *briefly* drying them by passing an Ar stream over them with a slight vacuum. Loss of NO from the crystals, clearly observable as decolorization, was facile and application of too much vacuum or purging with too much Ar caused rapid decomposition. The collected crystals were quickly transferred into a glovebox in a sealed flask under a very slight vacuum so they could be handled and stored (-20 °C; 205 mg, 68% crude yield of $1 \cdot C_7H_8$). Our inability to collect **1** as a dry solid free of solvent without the inevitable loss of some NO has prevented acquisition of an acceptable elemental analysis thus far. $Tp^{t\text{-Bu}}\text{Cu}^{15}\text{NO}$ was prepared in the same way, except a slight excess of ^{15}NO gas was directly vacuum transferred into the reaction flask. The product could also be obtained by using $Tp^{t\text{-Bu}}\text{Cu}(\text{CH}_3\text{CN})$ (171 mg, 0.352 mmol) as the starting material, but yields were slightly lower (65 mg, 38% crude yield of $1 \cdot C_7H_8$). For X-ray crystallographic experiments, the reaction flask was immersed in an ice bath and opened, the solvent was quickly removed by pipet, and heavy-weight oil was immediately added to coat the crystals in order to inhibit solvent and NO loss. A suitable crystal was then chosen and mounted under a cold (-101 °C) N_2 stream on the diffractometer. Stoichiometry of solvate inclusion in the crystals was determined by X-ray crystallography for both toluene and mesitylene, although in the case of $S =$ toluene (data not shown) extreme disorder problems prevented accurate modeling of the critical CuNO unit. For most spectroscopic work, Cu(I) starting material solutions of known

concentration were prepared in sealed vials, the vials were purged with NO gas with vigorous shaking, and then the solutions were directly transferred to the appropriate NO-purged spectroscopic cell with a gas-tight syringe. Samples for spectroscopy could also be prepared directly by dissolving isolated crystals of **1 · nS** in appropriate solvents, but these often bleached rapidly due to NO loss (identified by GC). FTIR (KBr) 2963, 2481 [v(BH)], 1712 [v(¹⁴NO); v(¹⁵NO) = 1679], 1505, 1362, 1202, 1165, 1052, 774, 735 cm⁻¹.

Tp^{Ph2CuNO (2)}. Tp^{Ph2Cu(3,5-Ph₂pz)} (230 mg, 0.241 mmol) was dissolved in 2 mL toluene in a Schlenk flask and hexanes (1.0 mL) was added. The flask was purged with NO gas, with vigorous shaking, until the solution turned dark orange. Bright orange crystals of **2** formed upon allowing the solution to stand for 1-2 days at -20 °C. Collection of crystals was as in **1** above, and was additionally hampered by the concomitant crystallization of 3,5-Ph₂pz (201 mg crude weight). Again, we were unable to collect the product as a dry solid free of solvent or small amounts of 3,5-Ph₂pz and thus we have not obtained a satisfactory elemental analysis. Tp^{Ph2Cu¹⁵NO} was prepared in the same way, except a slight excess of ¹⁵NO gas was directly vacuum transferred into the reaction flask. Solutions of **2** could also be formed by treating a solution of Tp^{Ph2Cu(CH₃CN)} with NO, but crystals were not isolated in this instance. Freshly prepared solutions of [Tp^{Ph2Cu}]₂ were unreactive with NO, but upon standing for several hours **2** slowly appeared (UV-Vis spectroscopy). Samples for spectroscopy were prepared as described above for **1**. FTIR (KBr): 3062, 2624 [v(BH)], 1720 [v(¹⁴NO); v(¹⁵NO) = 1687] 1544, 1478, 1462, 1363, 1340, 1262, 1233, 1169, 1072, 1010, 805, 761, 696, 568 cm⁻¹.

Reaction of 1 with O₂. (a) Excess NO present. A solution of **1** prepared by purging a solution of [Tp^{t-BuCu}]₂ (170 mg, 0.191 mmol) in CH₂Cl₂ (~15 mL) with NO was purged with O₂. The solution immediately became bright green. Evaporation of solvent under reduced pressure yielded a green precipitate. EPR spectroscopic analysis of a solution of this precipitate in 1:1 CH₂Cl₂/toluene indicated that Tp^{t-BuCu(NO₃)} was

the only EPR-detectable species present (43% of crude product mass by integration). The remaining mass is presumably the as yet uncharacterized EPR silent product that results from the reaction of $[Tp^{t\text{-Bu}}\text{Cu}]_2$ with O_2 .²⁹ Crystals of $Tp^{t\text{-Bu}}\text{Cu}(\text{NO}_3)$ which exhibited identical spectroscopic properties to those reported in the literature²⁶ were obtained by reacting $[Tp^{t\text{-Bu}}\text{Cu}]_2$ (55 mg, 0.06 mmol) with NO in THF (1 mL), purging with O_2 , and then adding MeOH (5 mL) dropwise (19 mg, 31%). **(b) Excess NO minimized.** A solution of **1** prepared as described above was frozen by immersion of the reaction flask in a liquid N_2 bath, the head space was evacuated, and a slight excess of O_2 was added via vacuum transfer. Upon warming, the solution turned green-yellow. EPR spectroscopic analysis of the precipitate resulting from removal of solvent from the reaction solution in 1:1 CH_2Cl_2 /toluene indicated the presence of $Tp^{t\text{-Bu}}\text{Cu}(\text{NO}_2)$,²⁸ $Tp^{t\text{-Bu}}\text{Cu}(\text{NO}_3)$, and a small amount of an unidentified species with an axial signal.

Reaction of 1 and 2 with CO. Flushing solutions of **1** or **2** in toluene with CO (1 atm) resulted in quantitative conversion to $Tp^{t\text{-Bu}}\text{CuCO}$ or $Tp^{\text{Ph}2}\text{CuCO}$, respectively, according to comparisons of ^1H NMR spectra of the white solids obtained upon solvent removal with literature data ($Tp^{\text{Ph}2}\text{CuCO}$)²⁴ or with that of an independently prepared sample ($Tp^{t\text{-Bu}}\text{CuCO}$). The latter complex was prepared as follows. $[Tp^{t\text{-Bu}}\text{Cu}]_2$ (0.090 g, 0.101 mmol) was stirred in toluene (5 mL) under 1 atm CO atmosphere for 5 min. The product was isolated by reducing the solvent volume to < 1 mL under reduced pressure and collecting the resulting white microcrystalline powder (0.082 g, 87%). ^1H NMR (300 MHz, CD_2Cl_2) δ 1.47 (s, 27 H), 6.07 (d, $J = 2.1$ Hz, 3 H), 7.51 (d, $J = 2.1$ Hz, 3 H) ppm; ^{13}C NMR (75 MHz, CD_2Cl_2) δ 30.9, 32.2, 101.5, 134.9, 162.4 ppm; IR (KBr) 735, 771, 1201, 1259, 1361, 1460, 1504, 2069 [$\nu(\text{CO})$], 2473 [$\nu(\text{BH})$], 2968 cm^{-1} ; Anal. Calcd for $\text{C}_{22}\text{H}_{34}\text{BCuN}_6\text{O}$: C, 55.88; H, 7.25; N, 17.78; Found: C, 55.31; H, 7.14; N, 17.48.

$Tp^{t\text{-Bu}}\text{CuCl}$ (3). A brief description of the synthesis of this compound has appeared^{26a} and its X-ray structure has been reported.^{26b} In an alternative synthesis, a

green solution of CuCl₂·2H₂O in methanol (88 mg, 0.51 mmol) was added to a solution of TiTp^t-Bu (266mg, 0.45mmol) in THF (10 mL). The mixture immediately turned brown and precipitate appeared. The solution was filtered, solvent was removed from the filtrate, and the residue was redissolved in THF (10 mL). The filtration procedure was repeated, except this time the volume of the filtrate was reduced in vacuo to <5 mL and MeOH (~1 mL) was added. The solution volume was then further reduced until crystals began to appear. More crystals formed upon standing at -20 °C. The brown crystals were collected by filtration and washed with methanol (139 mg, 64 %): FTIR (KBr): 2960, 2525 [v(BH)], 1497, 1394, 1364, 1341, 1260, 1297, 1167, 1101, 1056, 8774, 783, 731 cm⁻¹.

Tp^t-BuCuBr (4). This compound was prepared as described for 3, except CuBr₂ was used as the starting material and the solid that was obtained after the first evaporation was redissolved in CH₂Cl₂ instead of THF to ultimately afford burgundy crystals of 4 (155 mg, 58%). FTIR (KBr, cm⁻¹): 2961, 2483 [v (BH)], 1500, 1394, 1365, 1339, 1260, 1231, 1198, 1168, 1058, 920, 792, 732 cm⁻¹; Anal. Calcd. for C₂₁H₃₄BBrCuN₆: C, 48.06; H, 6.53; N, 16.01; Found: C, 47.62; H, 6.59; N, 16.07.

Tp^t-BuCuN₃ (5). In an inert atmosphere glovebox, excess TMSN₃ (~ 0.5 mL) was added to an aqua-green solution of Tp^t-BuCu(OAc) (330 mg, 0.65 mmol) in toluene (~5 mL). The solution immediately turned violet and crystals of 5 deposited upon allowing it to stand at -20 °C (270 mg, 85%): FTIR (KBr): 2960, 2492 [v(BH)], 2051 [v(N₃)], 1500, 1342, 1261, 1198, 1055, 790, 732 cm⁻¹; Anal. Calcd for C₂₁H₃₄BCuN₉: C, 51.81; H, 7.04; N, 25.89; Found: C, 51.83; H, 7.00; N, 25.80.

Tp^t-BuCu(OTf) (6). The following procedure was found to be more efficient than that reported earlier.²⁷ In an inert atmosphere glovebox, excess TMSOTf (~0.3 mL) was added to a solution of Tp^t-BuCu(OAc) (127 mg, 0.25 mmol) in toluene (~4 mL). The solution immediately turned black and crystals began to form. After allowing the mixture to stand at -20 °C for 3-4 hours, the black-purple crystals of 6 were collected by

filtration and washed with a small amount of (<1 mL) toluene (116 mg, 68%). Spectroscopic data for samples prepared in this manner exactly matched those which were reported previously.²⁷

X-Ray Crystal Structure of $\text{Tp}^{t\text{-Bu}}\text{CuNO} \cdot 0.5 \text{ C}_9\text{H}_{12}$ (1). A red plate-shaped crystal of dimensions $0.60 \times 0.50 \times 0.40$ mm was mounted on a glass fiber with heavy weight oil and quickly placed under a cold N_2 stream on the diffractometer. Measurements were made on an Enraf-Nonius CAD-4 diffractometer with graphite monochromated $\text{MoK}\alpha$ ($\lambda = 0.71073 \text{ \AA}$) radiation. Important crystallographic information is summarized in Table IV. Cell constants were obtained from a least squares refinement of the setting angles of 25 carefully centered reflections in the range $28.2 < 2\theta < 36.0^\circ$. Although the cell dimensions suggested an orthorhombic unit cell, the Laue symmetry, $2/m$, indicated a monoclinic cell. The intensity data were collected using the ω - 2θ scan technique to a maximum 2θ value of 50.2° . An empirical absorption correction was applied, using the program DIFABS,⁶⁶ which resulted in transmission factors ranging from 0.81 to 1.20. The data were corrected for Lorentz and polarization effects, but no decay correction was needed. The non-hydrogen atoms of 1 were refined anisotropically, and the crystallization solvent atoms were refined isotropically. The structure was solved by direct methods⁶⁷ using the TEXSAN⁶⁸ software package. Neutral atom scattering factors⁶⁹ and anomalous dispersion terms⁷⁰ were taken from the literature. For 3399 unique, observed reflections with $I > 2\sigma(I)$ and 287 variables, least squares refinement converged with unsatisfactory values for the discrepancy indices R and R_w of 0.128 and 0.155, respectively, due to twinning that was estimated⁷¹ to be 10-15% from the pattern of observed intensities of pairs of reflections hkl and $hk-l$. In the absence of any untwinned crystals, refinements continued with the program CRYSTALS (Chemical Crystallography Laboratory, Oxford University, Oxford, England), where the function now minimized was $\sum_{hkl} w(hkl)[|F_o(hkl)| - |F_c(hkl)|]^2$ with calculated structure factors $F_c(hkl)$ that included contributions from the twin

elements as $|F_c(hkl)| = [\alpha |F_c(hkl)|^2 + (1-\alpha) |F_c(hk-l)|^2]^{1/2}$. Weights, $w(hkl)$ were derived from a 3-term Chebyshev polynomial fit to the residuals prior to the last two cycles of refinement. Least-squares refinements converged smoothly to values for R and R_w of 0.0519 and 0.0653 for 2866 reflections having $I > 3\sigma(I)$ for a model described by 293 variable parameters. The value of α for the primary twin was 0.8477 (16). The mesitylene solvate molecule, which is disordered near a center of inversion, was treated as a rigid group of standard geometry. Hydrogen atoms were included as a fixed contribution to F_c at their calculated idealized positions. Internal consistency among chemically equivalent bond distances and angles of the three 3-*t*-butylpyrazolyl groups is in accord with that expected from the estimated standard deviations, as obtained from the inverse least-squares matrix, for individual bond parameters. Anisotropic displacement parameters are normal for all atoms. Although these are higher for the nitrosyl oxygen atom, the closest non-bonded contact that this oxygen atom makes is 3.58 Å with a *t*-butyl carbon atom and there is no evidence for disorder in the coordinated nitrosyl moiety. The final difference Fourier map is flat and featureless, with maximum and minimum peaks of 0.33 e⁻/Å³ and -0.39 e⁻/Å³, respectively. ORTEP drawings of the structure with selected bond lengths and angles noted appear in Figure 3. Final atomic positional parameters and $B(\text{eq})$ values (excluding H atoms and atoms of solvent) are listed in Table V. A fully labeled ORTEP diagram and full tables of bond lengths and angles, atomic positional parameters, and final thermal parameters for nonhydrogen atoms are given in the supplementary material from the preliminary communication of this structure.²¹

Theoretical Methods. Unrestricted Hartree-Fock calculations were performed for the Cu(NH₃)₃NO radical cation using a double zeta quality basis set for H [4s | 2s],⁷² N, O [9s4p1d | 4s2p1d],⁷² and Cu [13s10p5d | 5s4p2d].⁷³ The Cu–N and N–O bond lengths were chosen from the crystal structure of **1**, as was the Cu–N–O bond angle. The N(O)–Cu–N angles were all set to the average crystal structure angle of 123.1°. The

ammonia groups were chosen to be locally C_{3v} symmetric about the Cu–N axis, with N–H bond lengths of 1.0 Å and Cu–N–H bond angles of 110°. Configuration interaction including all single and double excitations (CISD) was performed for the lowest energy $^2A'$ wavefunction with the core orbitals frozen to substitution. Configuration interaction including all single substitutions (CIS) was performed for this state in order to calculate the first six excited state transitions.⁴⁶

Isotropic hyperfine coupling constants were obtained from equation 2, where g (g_X) is the electronic (nuclear) g value and β (β_X) is the Bohr (nuclear) magneton. The Fermi contact integral, $\rho(X)$, is defined in equation 3 where $P^{\alpha-\beta}$ is the calculated one-electron spin density matrix, the basis functions ϕ are evaluated at the nuclear coordinates, and the sum is over basis set orbital indices.^{74,75} The exact CISD spin density matrix was calculated employing the Z-vector method of Handy and Schaefer.⁷⁶

$$\alpha_X = (8\pi/3)gg_X\beta\beta_X\rho(X) \quad (2)$$

$$\rho(X) = \sum_{\mu\nu} P_{\mu\nu}^{\alpha-\beta} \phi_\mu(R_X) \phi_\nu(R_X) \quad (3)$$

As the expectation values for the total spin operator, $\langle S^2 \rangle$, were 0.766 and 0.767 for the $^2A'$ and $^2A''$ HF wavefunctions respectively, spin contamination should not affect these calculations significantly. All calculations were performed with the Gaussian 92 program suite.⁷⁷ Orbital plots (Figure 8) were generated using the AVS Chemistry Viewer version 1.5 on a Stardent/Kubota Titan 3040.

Acknowledgements. We thank Professor Doyle Britton (University of Minnesota) for his work on the X-ray structure of **1**, Professor Geoffrey Jameson (Georgetown University) for solving the twinning problem with the X-ray data for **1**, Professor John

Lipscomb (University of Minnesota) for providing access to his EPR facility and simulation program, Mei Whittaker and Greg Landrum (Carnegie Mellon University) for their assistance in obtaining MCD and near-IR spectra, and Douglas A. Smith and Charles W. Ulmer II for generating the orbital plots. Financial support was provided by the Exxon Education Foundation (W.B.T.), the National Institutes of Health (GM47365 to W.B.T. and GM46749 to J.W.W.), the National Science Foundation (DMB-9105519 to W.E.A.), the Searle Scholars Program/Chicago Community Trust (W.B.T.), the National Biomedical ESR Center in Milwaukee (RR01008), an NSF Equipment Grant (CHE 78-23857) for the Cary 17D Near-IR spectrophotometer, and the University of Minnesota.

References

1. Richter-Addo, G. B.; Legzdins, P. *Metal Nitrosyls*; Oxford University Press: New York, 1992.
2. (a) Kroneck, P. M. H.; Beuerle, J.; Schumacher, W. In *Degradation of Environmental Pollutants by Microorganisms and their Metalloenzymes*; H. Sigel and A. Sigel, Ed.; Metal Ions in Biological Systems; Marcel Dekker: New York, 1992; Vol. 28; pp 455-505. (b) Kroneck, P. M. H.; Zumft, W. G. In *Denitrification in Soil and Sediment*; N. P. Revsbech and J. Sorensen, Ed.; Plenum Press: New York, 1990; pp 1-20. (c) Stouthamer, A. H. In *Biology of Anaerobic Microorganisms*; A. J. B. Zehnder, Ed.; Wiley: New York, 1988; pp 245-301. (d) Zumft, W. G.; Viebrock, A.; Korner, H. In *The Nitrogen and Sulphur Cycles*; J. A. Cole and S. J. Ferguson, Ed.; Cambridge University Press: Cambridge, MA, 1988; pp 245-280. (e) Hochstein, L. I.; Tomlinson, G. A. *Ann. Rev. Microbiol.* 1988, 42, 231-261. (f) *Denitrification, Nitrification, and Atmospheric Nitrous Oxide*; Delwiche, C. C., Ed.; John Wiley & Sons: New York, 1981.

3. (a) Weeg-Aerssens, E.; Tiedje, J. M.; Averill, B. A. *J. Am. Chem. Soc.* **1988**, *110*, 6851-6856. (b) Kim, C.-H.; Hollocher, T. C. *J. Biol. Chem.* **1984**, *259*, 2092-2099. (c) Garber, E. A. E.; Hollocher, T. C. *J. Biol. Chem.* **1982**, *257*, 8091-8097. (d) Goretski, J.; Hollocher, T. C. *J. Biol. Chem.* **1990**, *265*, 889-895. (e) Carr, G. J.; Ferguson, S. J. *Biochem. J.* **1990**, *269*, 423-429. (f) Carr, G. J.; Page, M. D.; Ferguson, S. J. *Eur. J. Biochem.* **1989**, *179*, 683-692. (g) Heiss, B.; Frunzke, K.; Zumft, W. G. *J. Bacteriol.* **1989**, *171*, 3288-3297. (h) Zafiriou, O. C.; Hanley, Q. S.; Snyder, G. J. *Biol. Chem.* **1989**, *264*, 5694-5699.
4. (a) Ye, R. W.; Toro-Suarez, I.; Tiedje, J. M.; Averill, B. A. *J. Biol. Chem.* **1991**, *266*, 12848-12851. (b) Hulse, C. L.; Averill, B. A.; Tiedje, J. M. *J. Am. Chem. Soc.* **1989**, *111*, 2322-2323. (c) Jackson, M. A.; Tiedje, J. M.; Averill, B. A. *FEBS Letters* **1991**, *291*, 41-44.
5. (a) Godden, J. W.; Turley, S.; Teller, D. C.; Adman, E. T.; Liu, M. Y.; Payne, W. J.; LeGall, J. *Science* **1991**, *253*, 438-442. (b) Adman, E.T.; Turley, S. In *Bioinorganic Chemistry of Copper*; K. D. Karlin and Z. Tyeklár, Ed.; Chapman & Hall, Inc.: New York, 1993; pp 397-405.
6. Libby, E.; Averill, B. A. *Biochem. Biophys. Res. Commun.* **1992**, *187*, 1529-1535.
7. (a) Solomon, E. I.; Lowery, M. D. *Science* **1993**, *259*, 1575-1581. (b) Solomon, E. I.; Baldwin, M. J.; Lowery, M. D. *Chem. Rev.* **1992**, *92*, 521-542.
8. (a) Fanning, J. C. *Coord. Chem. Rev.* **1991**, *110*, 235-73. (b) Waleh, A.; Ho, N.; Chantranupong, L.; Loew, G. H. *J. Am. Chem. Soc.* **1989**, *111*, 2767-2772. (c) Choi, I.-K.; Liu, Y.; Feng, D.; Paeng, K.-J.; Ryan, M. D. *Inorg. Chem.* **1991**, *30*, 1832-1839. (d) Hu, S.; Kincaid, J. R. *J. Am. Chem. Soc.* **1991**, *113*, 2843-2850. (e) Ozawa, S.; Fujii, H.; Morishima, I. *J. Am. Chem. Soc.* **1992**, *114*, 1548-1554.
9. (a) Zhang, Y.; Pavlosky, M. A.; Brown, C. A.; Westre, T. W.; Hedman, B.; Hodgson, K. O.; Solomon, E. I. *J. Am. Chem. Soc.* **1992**, *114*, 9189-9191. (b) Chen, V. I.; Orville, A. M.; Harpel, M. R.; Frolik, C. A.; Surerus, K. K.; Münck, E.;

- Libscomb, J. D. *J. Biol. Chem.* **1989**, *264*, 21677. (c) Hyman, M. R.; Seefeldt, L. C.; Morgan, T. V.; Arp, D. J.; Mortenson, L. E. *Biochemistry* **1992**, *31*, 2947-2955.
10. (a) Fraser, R. T. M. *J. Inorg. Nucl. Chem.* **1961**, *17*, 265-272. (b) Mercer, M.; Fraser, R. T. M. *J. Inorg. Nucl. Chem.* **1963**, *25*, 525-534. (c) Doyle, M. P.; Siegfried, B.; Hammond, J. J. *J. Am. Chem. Soc.* **1976**, *98*, 1627-1629.
11. (a) Paul, P. P.; Tyeklar, Z.; Farooq, A.; Karlin, K. D.; Liu, S.; Zubieta, J. *J. Am. Chem. Soc.* **1990**, *112*, 2430-2432. (b) Paul, P. P.; Karlin, K. D. *J. Am. Chem. Soc.* **1991**, *113*, 6331-6332.
12. (a) Gorren, A. C. F.; Boer, E. d.; Wever, R. *Biochim. Biophys. Acta* **1987**, *916*, 38-47. (b) Schoot Uiterkamp, A. J. M. *FEBS Lett.* **1972**, *20*, 93-96. (c) Schoot Uiterkamp, A. J. M.; Mason, H. S. *Proc. Natl. Acad. Sci. USA* **1973**, *70*, 993-996. (d) Wever, R.; Leeuwen, F. X. R. V.; Gelder, B. F. V. *Biochim. Biophys. Acta* **1973**, *302*, 236-239. (e) Schoot Uiterkamp, A. J. M.; Van der Deen, H.; Berendsen, H. C. J.; Boas, J. F. *Biochim. Biophys. Acta* **1974**, *372*, 407-425. (f) Rotilio, G.; Mosrurgo, L.; Graziani, M. T.; Brunori, M. *FEBS Lett.* **1975**, *54*, 163-166. (g) Van der Deen, H.; Hoving, H. *Biochemistry* **1977**, *16*, 3519-3525. (h) Van Leeuwen, X. R.; Gelder, B. F. V. *Eur. J. Biochem.* **1978**, *87*, 305-312. (i) Himmelwright, R. S.; Eickman, N. C.; Solomon, E. I. *Biochem. Biophys. Res. Commun.* **1978**, *81*, 237-242; **1979** *86*, 628-634. (j) Verplaetse, J.; Tornout, P. V.; Defreyn, G.; Witters, R.; Lontie, R. *Eur. J. Biochem.* **1979**, *95*, 327-331. (k) Brudvig, G. W.; Stevens, T. H.; Chan, S. I. *Biochemistry* **1980**, 5275-5285. (l) Martin, C. T.; Morse, R. H.; Kanne, R. M.; Gray, H. B.; Malmstrom, B. G.; Chan, S. I. *Biochemistry* **1981**, *20*, 5147-5155. (m) Spira, D. J.; Solomon, E. I. *Biochem. Biophys. Res. Commun.* **1983**, *112*, 729-736. (n) Boelens, R.; Rademaker, H.; Wever, R.; Gelder, B. F. V. *Biochim. Biophys. Acta* **1984**, *765*, 196-209. (o) Wever, R.; Boelens, R.; Boer, E. D.; Gelder, B. F. V.; Gorren, A. C. F.; Rademaker, H. *J. Inorg. Biochem.* **1985**, *23*, 227-232. (p) Suzuki, S.; Yoshimura, T.; Kohzuma, T.; Shidara, S.; Masuko, M.; Sakurai, T.; Iwasaki, H. *Biochem. Biophys. Res. Commun.* **1989**, *164*,

- 1366-1372. (q) Musci, G.; Marco, S. D.; di Patti, M. C. B.; Calabrese, L. *Biochemistry* **1991**, *30*, 9866-9872.
13. (a) Whittaker, M.M.; Whittaker, J.W. *Biophys. J.* **1993**, *64*, 762-772. (b) Whittaker, J.W. In *Bioinorganic Chemistry of Copper*; K. D. Karlin and Z. Tyeklár, Ed.; Chapman & Hall, Inc.: New York, 1993; pp 447-458.
14. (a) Giamello, E.; Murphy, D.; Magnacca, G.; Morterra, C.; Shioya, Y.; Nomura, T.; Anpo, M. *J. Catal.* **1992**, *136*, 510-520. (b) Iwamoto, M.; Yahiro, H.; Mizuno, N.; Zhang, W.-X.; Mine, Y.; Furukawa, H.; Kagawa, S. *J. Phys. Chem.* **1992**, *96*, 9360-9366. (c) Chao, C. C.; Lunsford, J. H. *J. Phys. Chem.* **1972**, *76*, 1546-1548. (d) Naccache, C.; Che, M.; Taarit, Y. B. *Chem. Phys. Lett.* **1972**, *13*, 109-112. (e) Anpo, M.; Nomura, T.; Kitao, T.; Gioamello, E.; Murphy, D.; Che, M.; Fox, M.A. *Res. Chem. Intermed.* **1991**, *15*, 225.
15. (a) Sato, S.; Yu-u, Y.; Yahiro, H.; Mizuno, N.; Iwamoto, M. *Appl. Catal.* **1991**, *70*, L1-L5. (b) Iwamoto, M.; Yahiro, H.; Tanda, K.; Mizuno, N.; Mine, Y.; Kagawa, S. *J. Phys. Chem.* **1991**, *95*, 3727-3730. (c) Li, Y.; Hall, W. K. *J. Catal.* **1991**, *129*, 202-215. (d) Li, Y.; Hall, W. K. *J. Phys. Chem.* **1990**, *94*, 6145-6148. (e) Anpo, M. In *Photochemical Conversion and Storage of Solar Energy*; E. Pelizzetti and M. Schiavello, Ed.; Kluwer Academic Publishers: Netherlands, 1991; pp 307-321.
16. *The Biology of Nitric Oxide*; Moncada, S.; Marletta, M. A.; Hibbs, J. B.; Higgs, E. A., Ed.; Portland Press: London, 1992; Vol. 1 and 2.
17. (a) Stuehr, D. J.; M. Ikeda-Saito *J. Biol. Chem.* **1992**, *267*, 20547-20550. (b) Boucher, J. L.; Genet, A.; Vadon, S.; Delaforge, M.; Mansuy, D. *Biochem. Biophys. Res. Commun.* **1992**, *184*, 1158-1164. (c) Boucher, J.-L.; Genet, A.; Vadon, S.; Delaforge, M.; Henry, Y.; Mansuy, D. *Biochem. Biophys. Res. Commun.* **1992**, *187*, 880-886. (d) Traylor, T. G.; Sharma, V. S. *Biochemistry* **1992**, *31*, 2847-2849. (e) Traylor, T. G.; Duprat, A. F.; Sharma, V. S. *J. Am. Chem. Soc.* **1993**, *115*, 810-811. (f) Christodoulou, D.; Maragos, C.M.; George, C.; Morley, D.; Dunams, T.M.; Wink,

- D.A.; Keefer, L.K. In *Bioinorganic Chemistry of Copper*; K. D. Karlin and Z. Tyeklár, Ed.; Chapman & Hall, Inc.: New York, 1993; pp 427-436.
18. Ignarro, L. J. *Biochem. Pharm.* **1991**, *41*, 485-490.
19. (a) Pellat, C.; Henry, Y.; Drapier, J.-C. *Biochem. Biophys. Res. Commun.* **1990**, *166*, 119-125. (b) Drapier, J.-C.; Pellat, C.; Henry, Y. *The J. Biol. Chem.* **1991**, *266*, 10162-10167. (c) Lancaster, J. R.; Hibbs, J. B. *Proc. Natl. Acad. Sci. USA* **1990**, *87*, 1223-1229. (d) Stadler, J.; Bergonia, H. A.; Silvio, M. D.; Sweetland, M. A.; Billiar, T. R.; Simmons, R. L.; J.R. Lancaster, J.; *Arch. Biochem. Biophys.* **1993**, *302*, 4-11. (e) Vanin, A. F.; Mordvintcev, P. I.; Hauschmidt, S.; Mülsch, A. *Biochim. Biophys. Acta* **1993**, *1177*, 37-42 and references therein.
20. For example, see T.D.Oury; Ho, Y.-S.; Piantadosi, C. A.; Crapo, J. D. *Proc. Natl. Acad. Sci. USA* **1992**, *89*, 9715-9719.
21. Carrier, S. M.; Ruggiero, C. E.; Tolman, W. B.; Jameson, G. B. *J. Am. Chem. Soc.* **1992**, *114*, 4407-4408.
22. Tolman, W. B.; Carrier, S. M.; Ruggiero, C. E.; Antholine, W. E.; Whittaker, J. W. In *Bioinorganic Chemistry of Copper*; K. D. Karlin and Z. Tyeklár, Ed.; Chapman & Hall, Inc.: New York, 1993; pp 406-418.
23. Carrier, S. M.; Ruggiero, C. E.; Houser, R. P.; Tolman, W. B. *Inorg. Chem.* in press.
24. Kitajima, N.; Fujisawa, K.; Fujimoto, C.; Moro-oka, Y.; Hashimoto, S.; Kitagawa, T.; Toriumi, K.; Tatsumi, K.; Nakamura, A. *J. Am. Chem. Soc.* **1992**, *114*, 1277-1291.
25. Fogg, P. G. T.; Gerrard, W. *Solubility of Gases in Liquids: A Critical Evaluation of Gas/Liquid Systems in Theory and Practice*; John Wiley & Sons: New York, 1992.
26. (a) Trofimenko, S.; Calabrese, J. C.; Thompson, J. S. *Inorg. Chem.* **1987**, *26*, 1507-1514. (b) Han, R.; Looney, A.; McNeill, K.; Parkin, G.; Rheingold, A. L.; Haggerty, B. S. *J. Inorg. Biochem.* **1993**, *49*, 105-121.

27. The X-band EPR spectrum of pure $\text{Tp}^t\text{-BuCu(NO}_3)$ in 1:1 CH_2Cl_2 /toluene at 77 K exhibits a characteristic multicomponent signal with both axial and rhombic features, implicating the presence of different structural isomers in solution.
28. Tolman, W. B. *Inorg. Chem.* **1991**, *30*, 4878-4880.
29. Carrier, S. M.; Ruggiero, C.E.; Tolman, W. B., unpublished results.
30. Kitajima, N.; Fujisawa, K.; Moro-oka, Y. *J. Am. Chem. Soc.* **1990**, *112*, 3210-3212.
31. (a) Feltham, R. D.; Enemark, J. H. *Top. Stereochem.* **1981**, *12*; 155-215. (b) Mingos, D. M. P.; Sherman, D. J. *Adv. Inorg. Chem.* **1989**, *34*, 293-377. (c) Enemark, J. H.; Feltham, R. D. *Coord. Chem. Rev.* **1974**, *13*, 339-406.
32. (a) Vänngård, T. In *Biological Applications of Electron Spin Resonance*; H. M. Swartz, J. R. Bolton and D. C. Borg, Ed.; Wiley-Interscience: New York, 1972; pp 411-447.
(b) Basosi, R.; Antholine, W. E.; Hyde, J. S. In *Biological Magnetic Resonance*; L. J. Berliner and J. Reubens, Ed.; Plenum Press: New York; Vol. 13; in press.
33. The relaxation process responsible for the temperature dependence of the EPR signal is under investigation: Koteiche, H.; Antholine, W.E.; Ruggiero, C.E.; Tolman, W.B., unpublished results.
34. Hathaway, B. J.; Billing, D. E. *Coord. Chem. Rev.* **1970**, *5*, 143-207.
35. (a) Lunsford, J. H. *J. Chem. Phys.* **1967**, *46*, 4347. (b) Lunsford, J. H. *J. Phys. Chem.* **1968**, *72*, 2141. (c) Ohigashi, H.; Kurita, Y. *J. Phys. Soc. Japan* **1968**, *24*, 654. (d) Lunsford, J.H. *J. Phys. Chem.* **1972**, *76*, 4163.
36. Brailsford, J. R.; Morton, J. R.; Vannotti, L. E. *J. Chem. Phys.* **1969**, *50*, 1051-1055.
37. Kitajima, N., personal communication.
38. Gewirth, A. A.; Cohen, S. L.; Schugar, H. J.; Solomon, E. I. *Inorg. Chem.* **1987**, *26*, 1133-1146.
39. Guss, J. M.; Merritt, E. A.; Phizackerley, R. P.; Hedman, B.; Murata, M.; Hodgson, K. O.; Freeman, H. C. *Science* **1988**, *241*, 806-11.
40. Brader, M. L.; Borchardt, D.; Dunn, M. F. *J. Am. Chem. Soc.* **1992**, *114*, 4480-4486.

41. Knapp, S.; Keenan, T. P.; Zhang, X.; Fikar, R.; Potenza, J.; Schugar, H. J. *J. Am. Chem. Soc.* **1990**, *112*, 3452-3464 and references therein.
42. Lever, A. B. P. *Inorganic Electronic Spectroscopy*; 2nd ed.; Elsevier: Amsterdam, 1984, Chapter 5.
43. (a) Pyrazole $\pi \rightarrow \text{Cu(II)} \text{ d}$ transitions in tetragonal complexes are known^{43b} to yield absorption features at significantly higher energy than the LMCT bands of 3-6, but the same factors that cause red-shifted $\text{d} \rightarrow \text{d}$ features in 3-6 (C_{3v} -distorted pseudotetrahedral geometry and low coordination number) would also be expected to cause lower energy LMCT absorptions. (b) Bernarducci, E.; Schwindinger, W. F.; J.L. Hughey, I.; Krogh-Jespersen, K.; Schugar, H. J. *J. Am. Chem. Soc.* **1981**, *103*, 1686-1691.
44. Gersten, B. S.; Brill, A. S.; *J. Chem. Phys.* **1985**, *82*, 1212-1230.
45. (a) Chipman, D. M. *Phys. Rev. A* **1989**, *39*, 475. (b) Poling, S. M.; Davidson, E. R.; Vincow, G. *J. Chem. Phys.* **1971**, *54*, 3005.
46. Foresman, J. B.; Head-Gordon, M.; Pople, J. A.; Frisch, M. J. *J. Phys. Chem.* **1992**, *96*, 135.
47. In C_s symmetry, a' orbitals are symmetric with respect to the symmetry plane, while a'' orbitals are anti-symmetric.
48. A study of TpZn(II) complexes at the PRDDO level of theory has appeared: Pavan Kumar, P. N. V.; Marynick, D. S. *Inorg. Chem.* **1993**, *32*, 1857.
49. For examples, see (a) Brockway, L. O.; Anderson, J. S. *Trans. Faraday Soc.* **1937**, *33*, 1233. (b) Albano, V. G.; Bellon, P.; Sansoni, M. *J. Chem. Soc., A* **1971**, 2420. (c) Berglund, D.; Meek, D. W. *Inorg. Chem.* **1972**, *11*, 1493.
50. (a) Couture, C.; Morton, J. R.; Preston, K. F.; Strach, S. J. *J. Magn. Res.* **1980**, *41*, 88-93. (b) Morton, J. R.; Preston, K. F.; Strach, S. J. *J. Phys. Chem.* **1980**, *84*, 2478-2481.

51. A broad and asymmetric EPR signal at g slightly less than 2.0 was observed for a frozen solution of NO at temperatures less than 30 K in the absence of the Cu(I) complexes.
52. Parker, W. L.; Crosby, G. A. *J. Phys. Chem.* **1989**, *93*, 5692-96.
53. (a) Schatz, P. N.; McCaffery, A. J. *Q. Rev., Chem. Soc.* **1969**, *23*, 552-584. (b) Dooley, D. M.; Dawson, J. H. *Coord. Chem. Rev.* **1984**, *60*, 1-66.
54. Salvato, B.; Giacometti, G. M.; Beltramini, M.; Zilio, F.; Giacometti, G.; Magliozzo, R. S.; Peisach, J. *Biochemistry* **1989**, *28*, 680-84.
55. Perin , D.D.; Armarego, W.L.F. *Purification of Laboratory Chemicals*; 3rd ed.; Pergamon: New York, 1988.
56. Lee, K. Y.; Kuchynka, D. J.; Kochi, J. K. *Inorg. Chem.* **1990**, *29*, 4196-4204.
57. Whittaker, J. W. ; W., M.M. *J. Am. Chem. Soc.* **1991**, *113*, 5528-5540.
58. Browett, W. R., Fucaloro, A.F., Morgan, T.V.; Stephens, P.J. *J. Am. Chem. Soc.* **1983**, *105*, 1868-1872.
59. Lipscomb, J. D. *Biochemistry* **1980**, *19*, 3590-3599.
60. (a) Froncisz, W.; Hyde, J. S. *J. Chem. Phys.* **1980**, *73*, 3123-3131. (b) Froncisz, W.; Hyde, J. S. *J. Magn. Res.* **1982**, *47*, 515-521.
61. Hyde, J. S.; Jesmanowicz, A.; Ratke, J. J.; Antholine, W. E. *J. Magn. Res.* **1992**, *96*, 1-13.
62. Aasa, R.; Värnngård, T. *J. Magn. Res.* **1975**, *19*, 308-315.
63. Courtesy of Professor John Lipscomb, Department of Biochemistry, University of Minnesota, Minneapolis, MN.
64. (a) Nigles, M. J.; Ph.D. Thesis, University of Illinois, Urbana, IL, 1979. (b) Maurice, A. M.; Ph.D. Thesis, University of Illinois, Urbana, IL, 1980.
65. Tolman, W. B.; Liu, S.; Bentsen, J. G.; Lippard, S. J. *J. Am. Chem. Soc.* **1991**, *113*, 152-164.
66. Walker, N.; Stuart, D. *Acta Crystallogr.* **1983**, *A39*, 158-166.

67. (a) Gilmore, C. J. *Appl. Cryst.* **1984**, *17*, 42-46. (b) Beurskens, P. T.; DIRDIF: Technical Report 1984/1; Thesis, Crystallography Laboratory: Toernooiveld, 6525 Ed Nijmegen, Netherlands, 1984.
68. TEXSAN-Texray Structure Analysis Package; Thesis, Molecular Structure Corp., 1985.
69. Cromer, D. T. *International Tables for X-ray Crystallography*; The Kynoch Press: Birmingham, United Kingdom, 1974; Vol. IV, Table I.2A.
70. (a) Ibers, J. A.; Hamilton, W. C. *Acta Crystallogr.* **1964**, *17*, 781. (b) Cromer, D. T. *International Tables for X-ray Crystallography*; The Kynoch Press: Birmingham, United Kingdom, 1974; Vol. IV, Table I.3.1.
71. Britton, D. *Acta Crystallogr. Sect. A*. **1972**, *28*, 296-297.
72. Dunning, T.H.; Hay, P.J. *Modern Theoretical Chemistry*; Plenum: New York, 1976.
73. (a) Wachters, A. J. H. *J. Chem. Phys.* **1970**, *52*, 1033. (b) Rappe, A. K.; Smedley, T. A.; Goddard, W. A. III *J. Phys. Chem.* **1981**, *85*, 2607.
74. (a) Weltner, W. *Magnetic Atoms and Molecules*, Scientific and Academic Editions: New York, 1983. (b) Symons, M. *Chemical and Biochemical Aspects of Electron Spin Resonance*, John Wiley & Sons: New York, 1978.
75. Using $g = 2.0$ and taking $C(X) = (8\pi/3)gg_x\beta\beta_X$ in units of Gauss: $C(^{63}\text{Cu}) = 423.8$, $C(^{17}\text{O}) = -216.6$, $C(^{15}\text{N}) = 161.8$, and $C(^{14}\text{N}) = 113.1$. See Koh, A. K.; Miller, D. J. *Atom. Data and Nucl. Data Tabl.* **1985**, *33*, 235.
76. Handy, N. C.; Schaefer, H. F., III, *J. Chem. Phys.* **1980**, *72*, 5031.
77. Frisch, M. J.; Trucks, G. W.; Head-Gordon, M.; Gill, P. M. W.; Wong, M. W.; Foresman, J. B.; Johnson, B. G.; Schlegel, H. B.; Robb, M. A.; Replogle, E. S.; Gomperts, R.; Andres, J. L.; Raghavachari, K.; Binkley, J. S.; Gonzalez, C.; Martin, R. L.; Fox, D. J.; Defrees, D. J.; Baker, J.; Stewart, J. J. P.; Pople, J. A. GAUSSIAN92, Gaussian, Inc., Pittsburgh PA, 1992.

Table I. EPR Parameters for NO and Isoelectronic N₂⁻ in Selected Environments.^a

Species	g _⊥	g	A _{⊥ Cu}	A _{Cu}	A _{⊥ N}	reference
1- ¹⁴ NO	1.99	1.83	62	107	27	this work
1- ¹⁵ NO	1.99	1.83	62	107	37	this work
2- ¹⁴ NO	2.00	1.84	61	107	28	this work
2- ¹⁵ NO	2.00	1.84	61	107	38	this work
Cu-NO in Y-type zeolite	2.009	1.89	178	212	—	15c
Cu-NO in ZSM5 zeolite	2.0053	1.87	165	164	—	15a
Cu-NO in Y-type zeolite	2.019	1.74	165	—	—	15d
Cu-NO in SrO ₂	2.030	1.94	112	166	—	15e
NO on MgO	1.996	1.89	—	—	30	35a
NO on ZnO	1.979	1.94	—	—	28	35b
NO on ZnS	1.997	1.91	—	—	29	35c
NO on NaY	1.898	1.86	—	—	25	35d
NO on decationated Y	1.996	1.95	—	—	—	35d
N ₂ ⁻ in KBr	2.00	1.88	—	—	20	36

^a Hyperfine coupling constants in cm⁻¹ × 10⁴.

Table II. EPR Parameters for $\text{Tp}^{\text{RR}'}\text{Cu(II)}X$ Complexes and Selected Biological Copper(II) Sites.

Species	$g_x (A_x)^a$	$g_y (A_y)^a$	$g_z (A_z)^a$	ref.
3	2.41^b	2.215^b	2.005 (98)	this work
4	2.46^b	2.19^b	2.01 (94)	this work
5	2.45^b	2.20^b	2.02 (74)	this work
6	2.36^b	2.13^b	2.02 (69)	this work
$\text{Tp}^{i\text{-Pr}_2}\text{CuCl}$	2.34 ^b	2.20 ^b	2.01 (97)	30
stellacyanin ^c	2.287 (35)	2.077 (29)	2.018 (57)	38
CBP ^d	2.207 (55)	2.08 (10)	2.02 (60)	39
$\text{Cu(II)}\text{-R}_6\text{-BT}^e$	2.230 (38)	2.090 (33)	2.025 (60)	40

^a Hyperfine coupling constants in $\text{cm}^{-1} \times 10^4$. ^b Signals not resolved sufficiently to allow unambiguous assignment of A values. ^c Values taken from simulations reported in ref. 40. ^d CBP = cucumber basic protein. ^e Cu(II)-R₆-BT = benzenethiolate complex of Cu(II)-substituted R-state insulin hexamer.

Table III. Electronic Absorption Spectroscopic Data for $\text{Tp}^{\text{RR}'}\text{Cu(II)}\text{X}$ Complexes in CH_2Cl_2 .

Complex	λ_{max} , nm (ϵ , $\text{M}^{-1} \text{cm}^{-1}$)	ref.
1	242 (10000), ^a 360 (2000), ^a 494 (1400)	this work
2	260 (22000), ^a 356 (3000), ^a 478 (1400)	this work
3	234 (6000), 292 (2100), 402 (1700), 474 (330) , 1030 (190)	this work
4	236 (4900), 260 (1700), 342 (1000), 484 (1800), 1090 (290)	this work
5	234 (7800), 292 (1500), 434 (350), 550 (350) , 1100 (93)	this work
6	234 (5600), 258 (2600), 286 (1600), 570 (2900) , 957 (390)	this work
$\text{Tp}^{\text{i-Pr}2}\text{CuCl}$	262 (1600), 362 (1900), 510 (310) , 996 (150)	30
$\text{Tp}^{\text{ii-Pr}2}\text{CuBr}$	334 (780), 445 (2300), 1053 (260)	30

^a These extinction coefficients are only crude approximations, due to the presence of overlapping features from the Cu(I) starting materials.

Table IV. Crystallographic Data for $\mathbf{1} \cdot 0.5\text{C}_9\text{H}_{12}$.

Formula	$\text{C}_{25.5}\text{H}_{40}\text{N}_7\text{BCuO}$
Formula wt (g mol⁻¹)	535.00
Space group	$\text{P}2_1/n$ (#14)
<i>a</i> , (Å)	10.28 (1)
<i>b</i> , (Å)	17.40 (2)
<i>c</i> , (Å)	16.12 (1)
β , (deg)	90.0 (1)
<i>V</i> (Å ³)	2882 (8)
<i>Z</i>	4
ρ_{calcd} (g cm ⁻³)	1.233
μ (cm ⁻¹)	7.87
temperature (°C)	-101
radiation, λ (Å)	MoK α , 0.71069
$2\theta_{\text{max}}$ (deg)	36.0
total no. of data collected	8575
total no. of unique data	4741
total no. unique data with $I > 3\sigma(I)$	2866
no. of variable parameters	293
R^{a}	.0519
R_w^{a}	.0653

^a $R = \sum | | F_o | - | F_c | | / \sum | | F_o | ; R_w = [(\sum w (| | F_o | - | F_c | |)^2 / \sum w | F_o |^2)]^{1/2}$, where $w = 4F_o^2/\sigma^2(F_o^2)$ and $\sigma^2(F_o^2) = [S^2(C + R^2B) + (pF_o^2)^2]/L_p^2$ with S = scan rate, C = total integrated peak count, R = ratio of scan time to background counting time, B = total background count, L_p = Lorentz-polarization factor, and p = p-factor (0.05).

Figure Captions

Figure 1. Schematic representation of the copper sites in nitrite reductase from *Achromobacter cycloclastes* (ref. 5).

Figure 2. UV-Vis absorption spectra of **1** and **2** in CH₂Cl₂.

Figure 3. ORTEP representations (40% probability ellipsoids, excluding solvate) of **1** · C₉H₁₂ (left) and its N₃CuNO core (right), with H atoms removed and only noncarbon atoms labeled for clarity. Selected bond angles not labeled on the core drawing (deg): N1-Cu1-N11, 124.3 (2); N1-Cu1-N21, 120.4 (2); N1-Cu1-N31, 124.6 (2); N11-Cu1-N21, 92.9 (4); N11-Cu1-N31, 93.4 (2); N21-Cu1-N31, 92.7 (2).

Figure 4. X (9.41 GHz)- and S (3.46 GHz)-band EPR spectra (top), first harmonics (middle), and current simulations (bottom) for frozen 1:1 CH₂Cl₂/toluene glasses of Tp^t-BuCu¹⁴NO (**1**-¹⁴NO) and Tp^t-BuCu¹⁵NO (**1**-¹⁵NO) at ~30 K.

Figure 5. X-band EPR spectra of **3** (a), **4** (b), **5** (c), and **6** (d) in 1:1 CH₂Cl₂/toluene at 77 K.

Figure 6. Electronic absorption spectrum of **1** in CH₂Cl₂ at ambient temperature (a) and MCD spectra of CD₂Cl₂ or CDCl₃ solutions at 4 K of **1** (b) and **2** (c). The weak signals at above 600 nm in the spectra of **1** are due to a Cu(II) impurity resulting from exposure to trace amounts of dioxygen during sample preparation.

Figure 7. Electronic absorption (top; in CH₂Cl₂) and MCD (bottom; in CD₂Cl₂) spectra of solutions of **3** at room temperature and 4 K, respectively.

Figure 8. Energies and graphical depictions of the UHF-calculated alpha frontier molecular orbitals for the simplified model compound $\text{Cu}(\text{NH}_3)_3\text{NO}^+$ (the LUMO, SOMO and predominantly copper d block MO's). The orientation of the molecule places the Cu-N-O plane orthogonal to the plane of the paper with the in-plane amine substituent in front, and the nitrosyl oxygen behind, the plane of the paper, respectively. Positive and negative orbital lobes are indicated as darker and lighter regions respectively. Note that the SOMO and LUMO are similar in terms of overall shape, but are oriented orthogonal to each other.

Figure 9. Qualitative molecular orbital diagram for 4-coordinate $\{\text{MNO}\}^{10}$ systems (adopted from ref. 31c). A similar diagram can be derived for the $\{\text{MNO}\}^{11}$ species **1** and **2** by breaking the degeneracy in the 4e orbital set and adding an additional electron to the lowest available orbital.

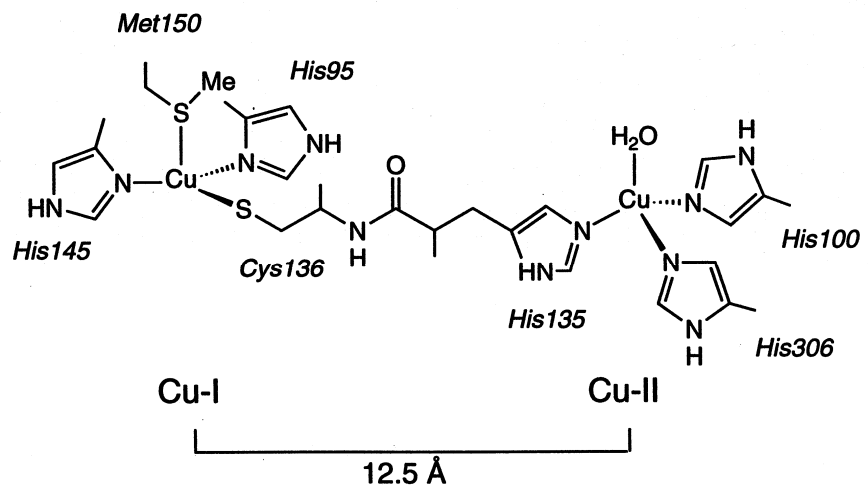


Figure 1 (Ruggiero et al.)

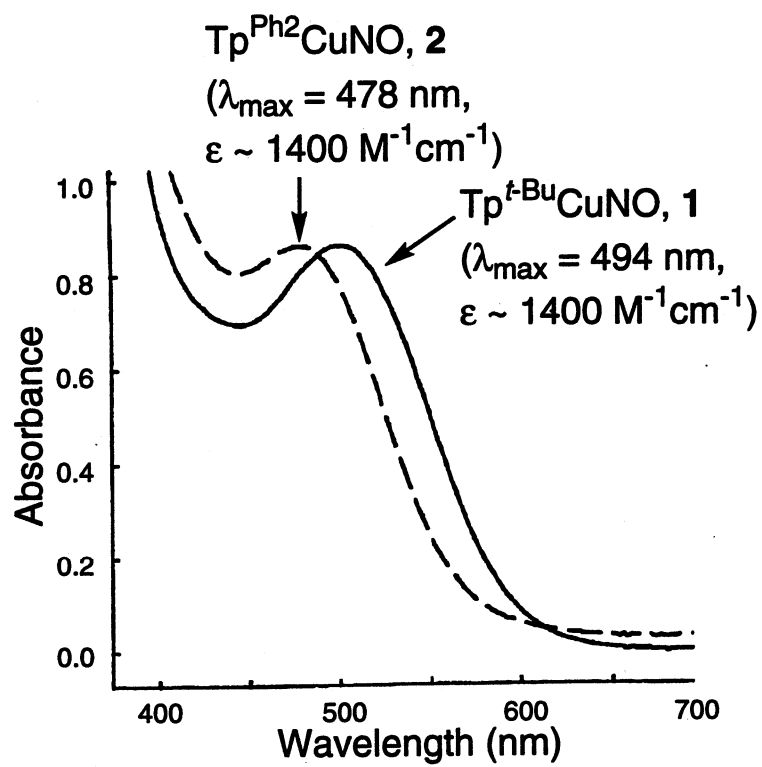


Figure 2 (Ruggiero et al.)

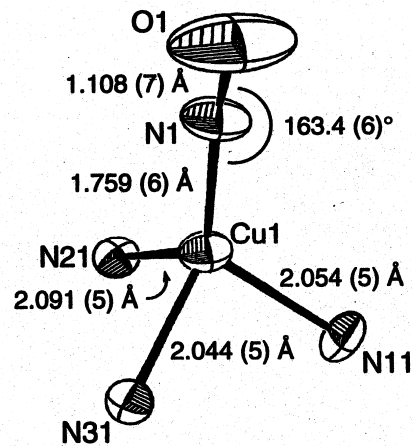
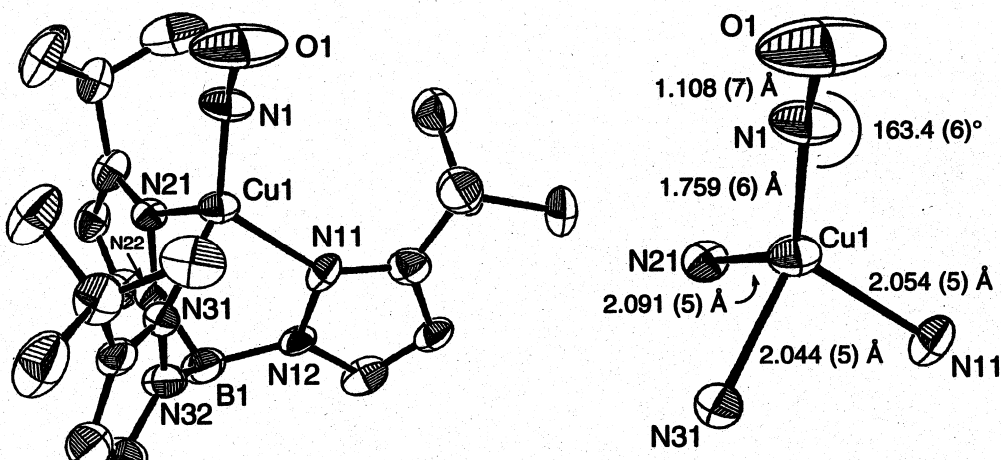


Figure 3 (Ruggiero et al.)

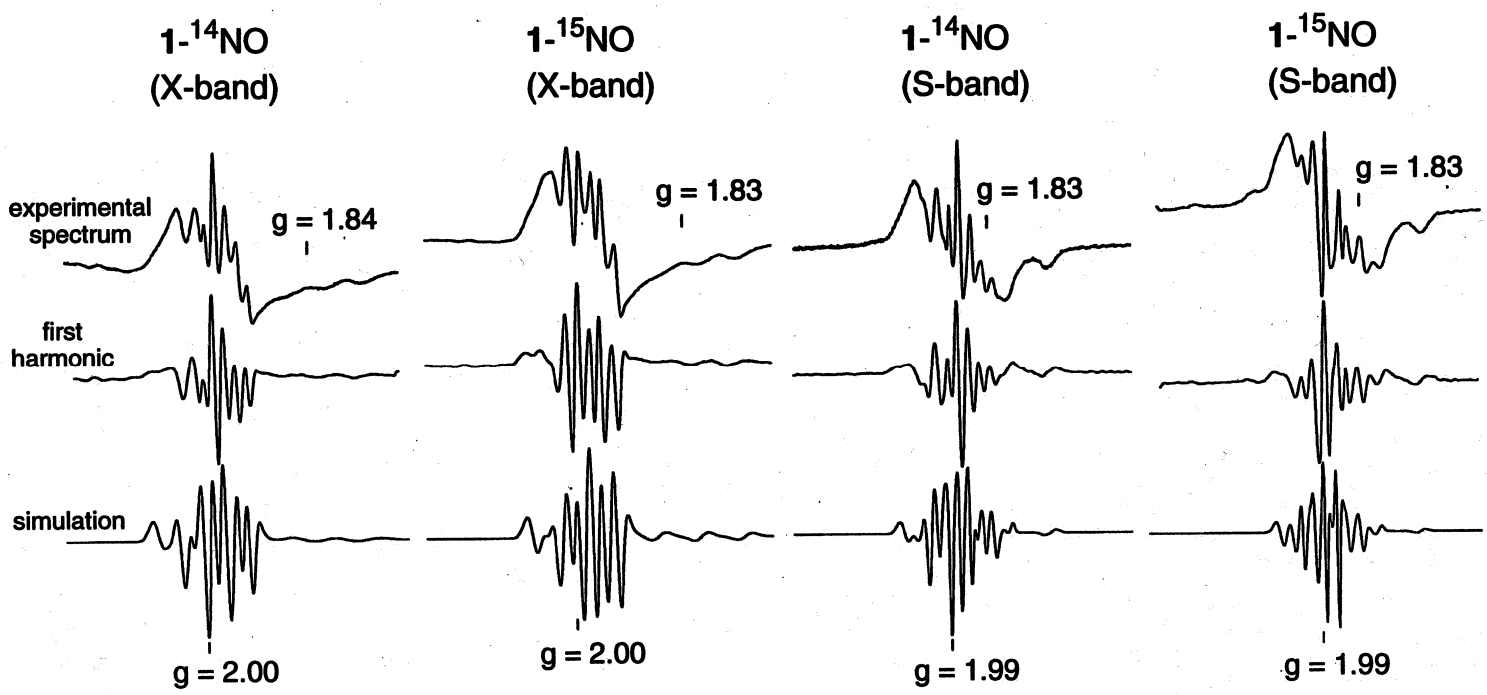


Figure 4 (Ruggiero et al.)

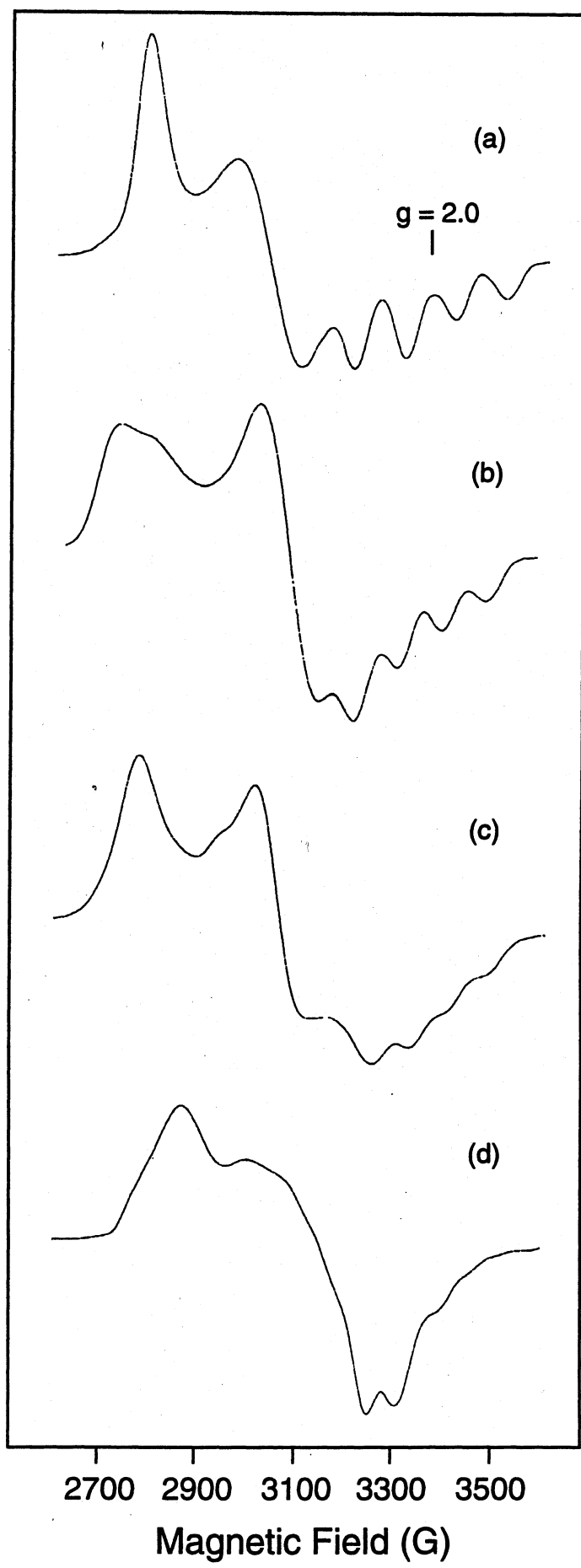


Figure 5 (Ruggier et al.)

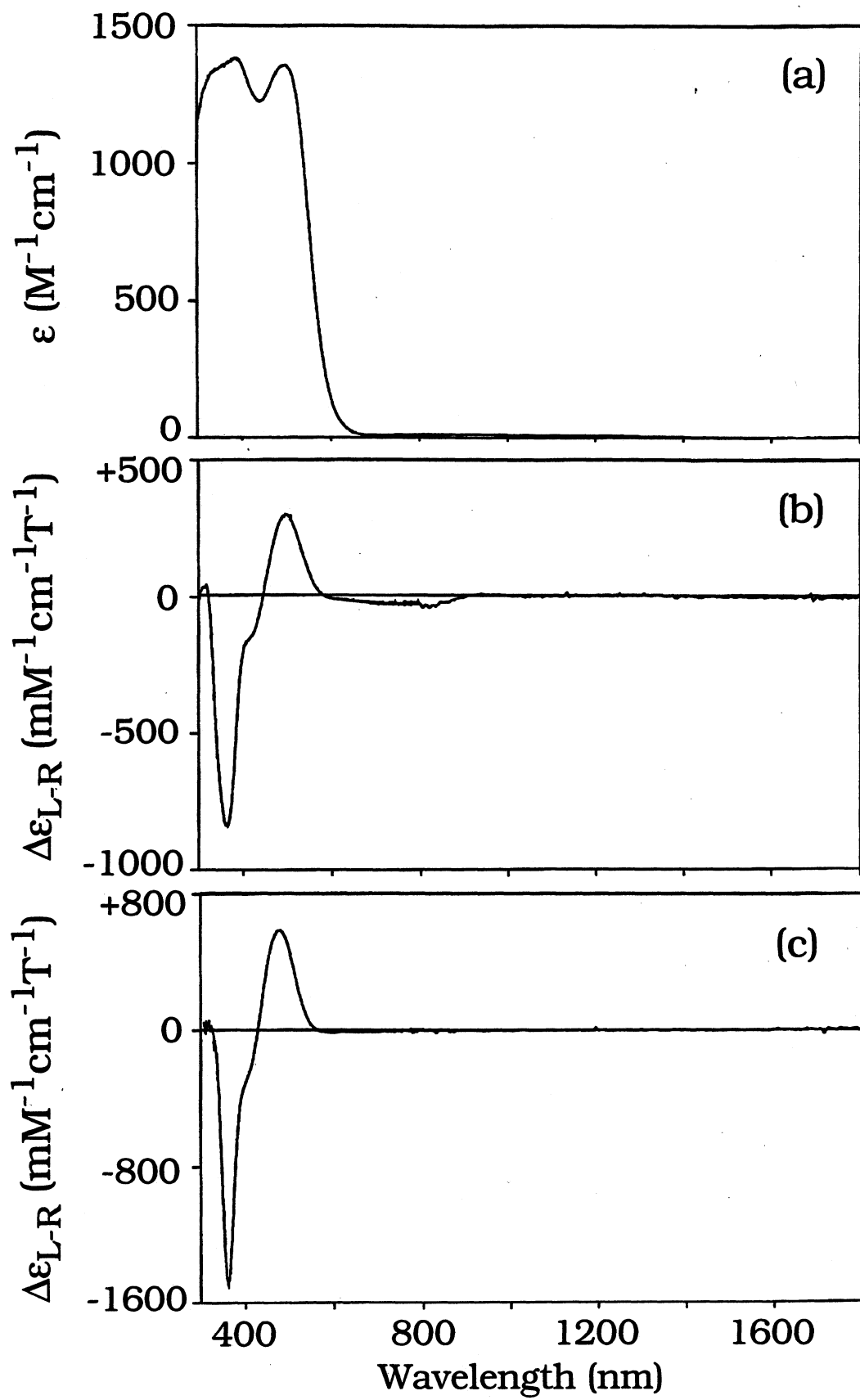


Figure 6 (Ruggiero et al.)

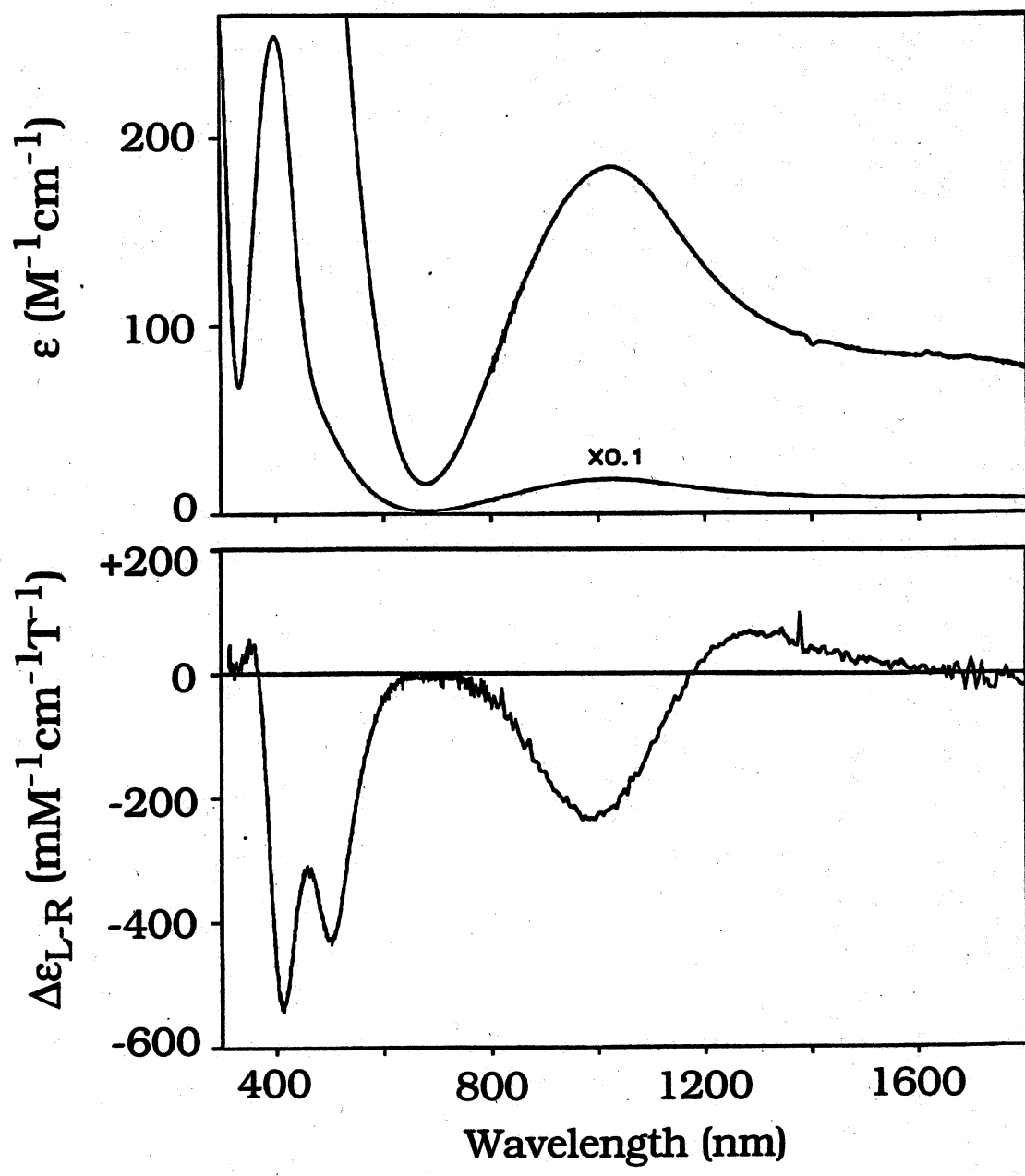


Figure 7 (Ruggiero et al.)

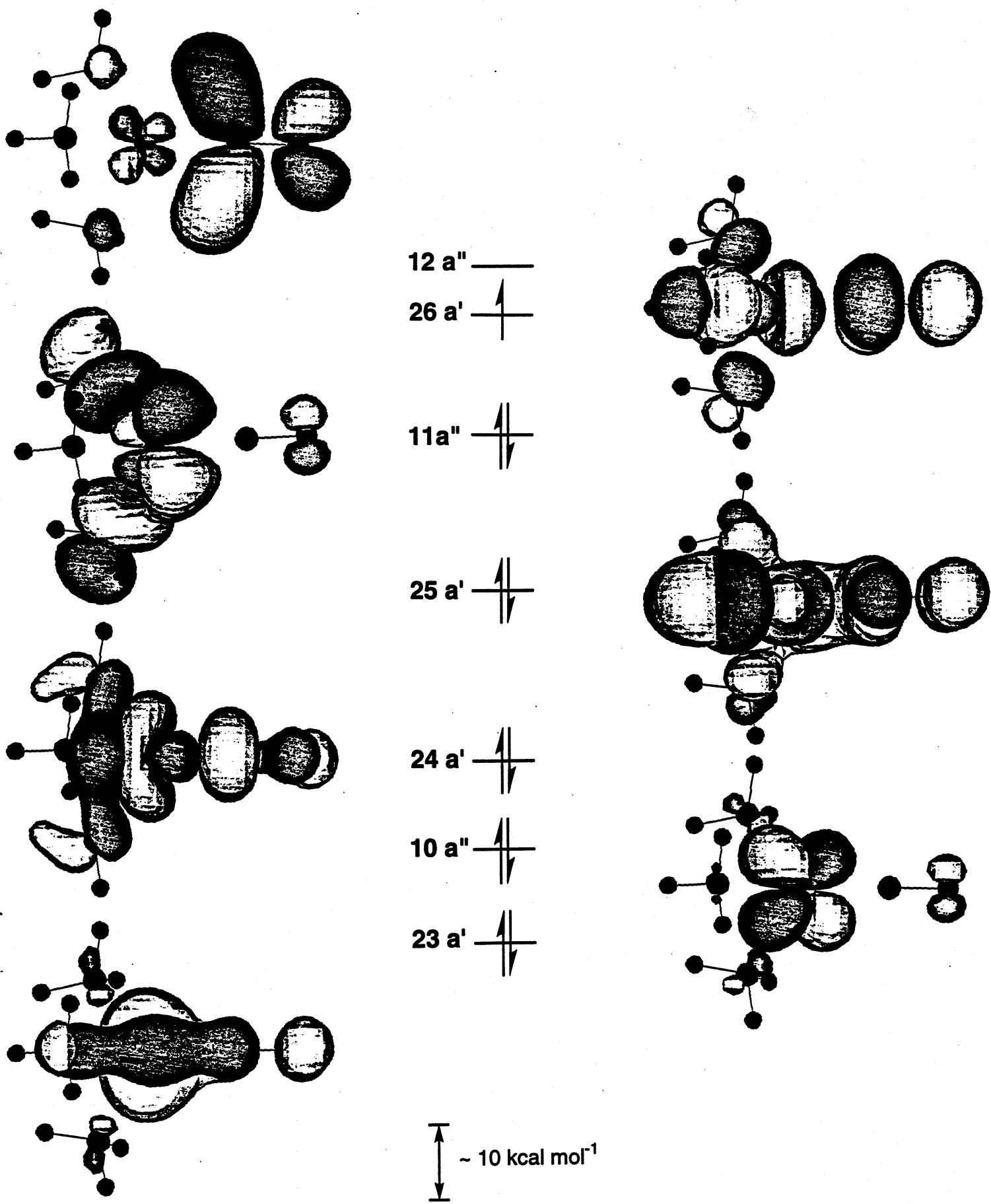


Figure 8 Ruggiero et al

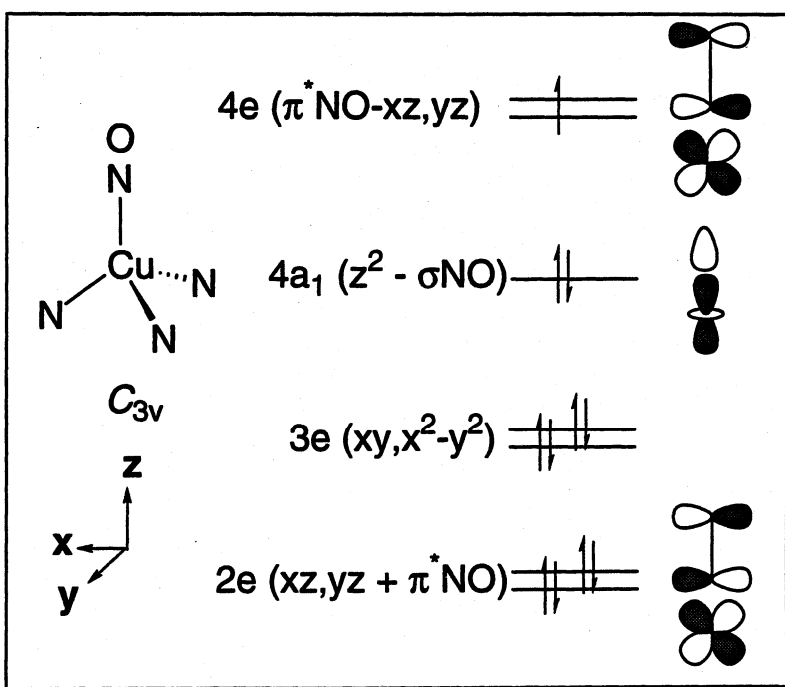
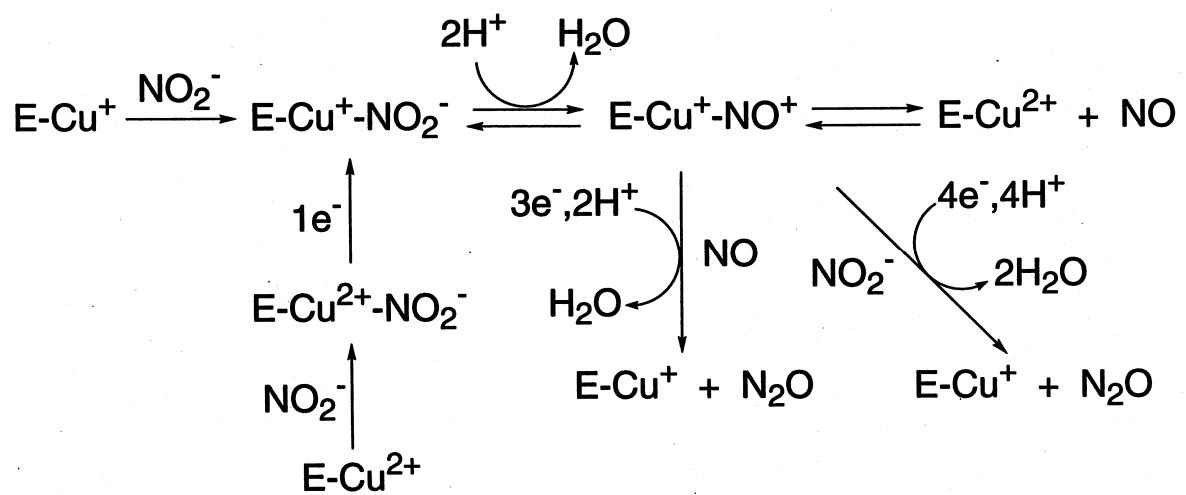
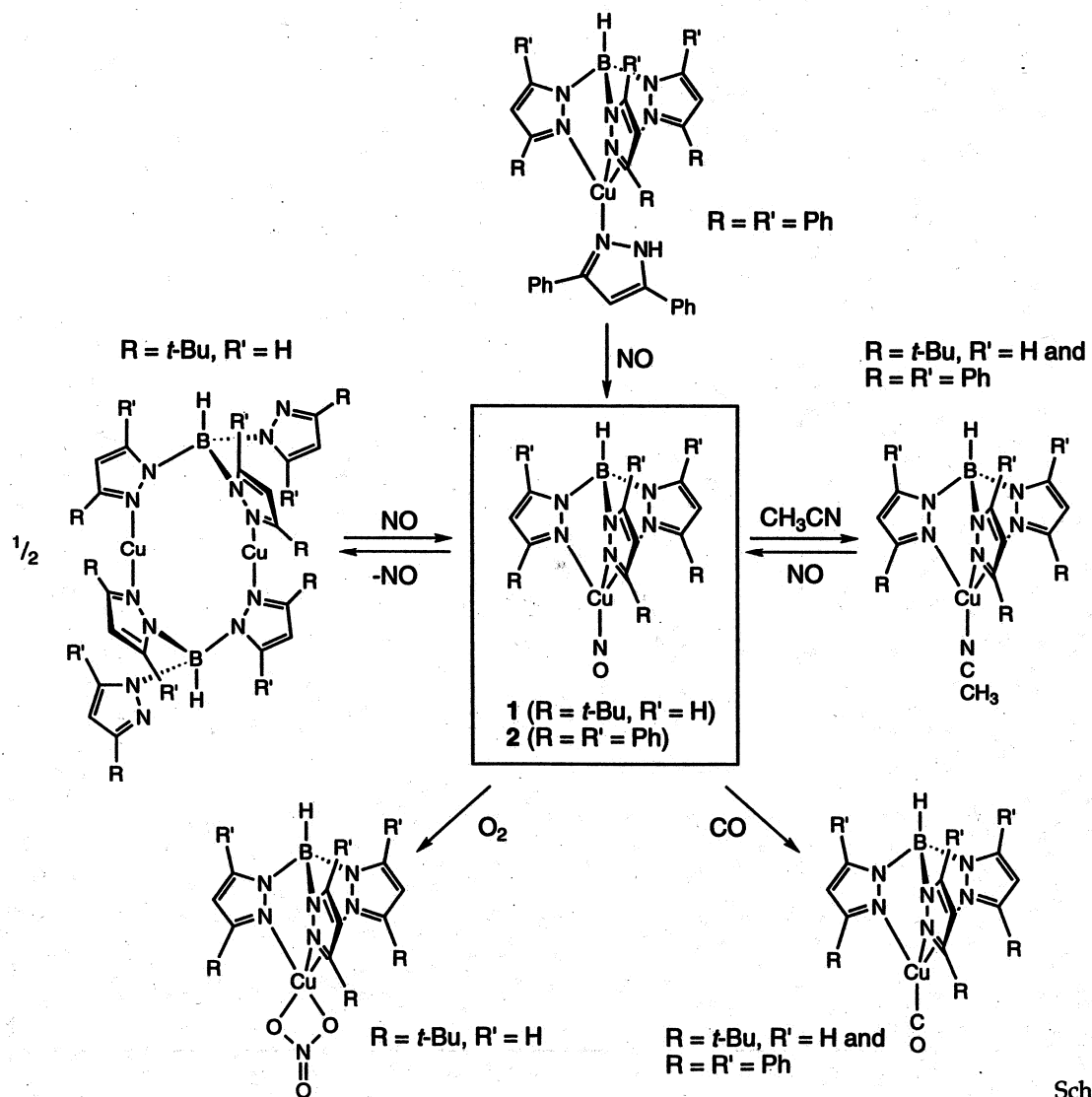


Figure 9 (Ruggiero et al.)



Scheme I (Ruggiero et al.)



Scheme II (Ruggiero et al.)